EVALUATION OF THE INTERGRANULAR COEFFICIENT OF FRICTION USING DISTINCT ELEMENT MODELLING

by

Yusuf Eşidir

B.S., Civil Engineering, Boğaziçi University, 2007

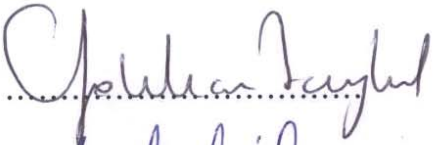
Submitted to the Institute for Graduate Studies in
Science and Engineering in partial fulfillment of
the requirements for the degree of
Master of Science

Graduate Program in Civil Engineering
Boğaziçi University
2009

EVALUATION OF THE INTERGRANULAR COEFFICIENT OF FRICTION USING DISTINCT ELEMENT MODELLING

APPROVED BY:

Assist. Prof. Özer Çinicioğlu ..... 
(Thesis Supervisor)

Prof. Gökhan Baykal ..... 

Assist. Prof. Kubilay Keleşoğlu ..... 

DATE OF APPROVAL: 27.01.2010

ACKNOWLEDGEMENTS

I would like to first thank my thesis supervisor Dr. Özer Çinicioğlu for his thoughtful guidance and support throughout the preparation of this thesis.

I extend my sincere thanks to Dr. Gökhan Baykal and Dr. Kubilay Keleşoğlu for their kind and supportive attitude towards me and their valuable advices.

I want to convey special thanks to Musa Rahmanlar and Murat Cenk Erdurak for their help during my experiments and during preparation of this thesis, and spending their invaluable time with me.

My deepest gratitude goes to my family members for their unflagging love and support throughout my life; this dissertation is simply impossible without them. During this work I have collaborated with many colleagues for whom I have great regard, Emin Çiftçi, Abdurrahman Ufuk Şahin, Tahir Erdem Öztürk, Hakkı Oral Özhan, and Egemen Danyıldız. Special thanks go to my dear friends Utku Soylu, Melih Savcı, and Arif Yılmaz for their motivation.

This thesis has been supported by Boğaziçi University Scientific Research Project BAP08A402.

ABSTRACT

EVALUATION OF THE INTERGRANULAR COEFFICIENT OF FRICTION USING DISTINCT ELEMENT MODELING

The shear strength of soil is generally expressed using macro-scale parameters, namely internal friction angle and cohesion. However this macro behavior is the resultant of dauntingly high number of intergranular interactions and the granular properties that control the mechanism of these interactions in the microscopic scale, such as granular size, shape, and surface texture.

The aim of this study is to understand the relationship between the friction angle of the continuum and the intergranular coefficient of friction. The behavior of the granular materials under shear is dependent on the properties of individual grains that are interacting with each other. Distinct element method considers these interactions and the governing laws are defined for the contacts of these individual grains. Therefore, computer simulations of the soil mechanics laboratory experiments using distinct element programs such as PFC2D will give a better understanding of phenomena at particle level. The micro-properties of granules can be identified in two scales; surface texture and surface shape. Surface texture is expressed by roughness of the grain and surface shape is expressed by roundness and sphericity. The coefficient of friction between interacting particles is mainly caused by the roughness of the grains. Physical measurement of roughness is not possible with known laboratory experiments, unless using specially developed measurement techniques. Therefore, intergranular coefficient of friction is an unknown parameter that can be investigated by numerical modeling.

For this purpose, numerical models of angle of repose test are created and coefficient of friction value is varied until the angle of repose in the DEM model matches the physical one. Different dry sand specimens according to their shape parameters and gradation are used in the laboratory experiments. Generating an initially compacted assembly at the desired porosity is problematic in numerical models when clumps are used

to reflect particle shapes. At this point, angle of repose test has an important advantage over other shear strength tests, such that there is no need to control porosity at the generation of initial assembly of particles. Therefore, porosity is not an initial condition for the angle of repose test.

As a result, experimental and numerical data are compared and conclusions are drawn about the value of interparticle coefficient of friction.

ÖZET

GRANÜLLER ARASI SÜRTÜNME KATSAYISININ AYRIK ELEMANLAR YÖNTEMİ KULLANILARAK BELİRLENMESİ

Zeminlerin kayma mukavemeti genelde içsel sürtünme açısı ve kohezyon gibi makro parametreler kullanılarak ifade edilir. Fakat bu makro davranış çok sayıda granül arasında oluşan etkileşimin ve bu etkileşimlerin mekanizmasını kontrol eden parçacık boyutu, şekli ve yüzey dokusu gibi özelliklerin bir sonucudur.

Bu çalışmanın amacı parçacıklar arası sürtünme katsayısı ile sürekli ortam sürtünme açısı arasındaki bağlantıya dair bir ilişki bulmaktır. Granüler malzemelerin kayma etkisi altındaki davranışı birbirleriyle etkileşim halinde olan münferit taneciklerin özelliklerine bağlıdır. Ayrık elemanlar yöntemi, bu etkileşimi göz önünde bulundurur ve bu yöntemde uygulanan kuramlar münferit taneciklerin temasları için tanımlanmıştır. Bu sebeple, PFC2D gibi ayrık elemanlar yöntemi ile çalışan bilgisayar programları kullanılarak hazırlanan zemin mekaniği deneylerinin numerik simülasyonları parçacık boyutundaki hadiselerin daha iyi anlaşılmasını sağlayabilir. Granüllerin mikro özellikleri, yüzey şekli ve yüzey dokusu olarak iki ölçekte değerlendirilebilir. Yüzey dokusu pürüzlülük ile, yüzey şekli ise yuvarlaklık ve küresellik ile ifade edilir. Birbirleriyle etkileşen parçacıklar arasındaki sürtünme katsayısı temelde granüllerin pürüzlülüğünden kaynaklanır. Pürüzlülüğün fiziksel ölçümü, duruma özel olarak geliştirilmiş bir yöntem kullanılmadıkça, bilinen laboratuar deneyleri ile mümkün değildir. Bu yüzden, parçacıklar arası sürtünme katsayısı, numerik modelleme açısından araştırılması gereken bilinmeyen bir parametredir.

Bu amaçla şev açısı deneyinin numerik modeli oluşturuldu ve sürtünme katsayısı değerleri ayrık elemanlar yöntemindeki şev açısı ile fiziksel şev açısı değerleri birbirleriyle örtüşene kadar denendi. Laboratuar deneylerinde, yüzey şekli özellikleri ve dane dağılımı açısından farklılıklar gösteren kuru kum numuneleri kullanıldı. Numerik modelin başlangıç aşamasında istenilen porozite değerinde sıkıştırılmış parçacık kümeleri oluşturmak

parçacık şekli öbeklerle (clump) tanımlandığında problemli bir durumdur. Bu noktada şev açısı deneyi, ilk olarak parçacık kümelerinin oluşturulması esnasında porozitenin kontrol altında tutulmasına gerek duyulmadığından, diğer kayma mukavemeti deneylerine kıyasla önemli bir avantaja sahiptir. Bu sebeple porozite, şev açısı deneyi için sağlanması gereken bir başlangıç koşulu değildir.

Netice itibarı ile bu çalışmada deneysel ve nümerik bulguların kıyaslanmasıyla parçacıklar arası sürtünme katsayısına dair sonuçlara varılmıştır.

TABLE OF CONTENTS

ACKNOWLEDGEMENTS iii
ABSTRACT iv
ÖZET vi
LIST OF FIGURES x
LIST OF TABLES xii
LIST OF SYMBOLS / ABBREVIATIONS xiii
1. INTRODUCTION 1
2. LITERATURE REVIEW 5
2.1. Introduction 5
2.2. Engineering Behavior and Strength of Dry Sand 5
2.3. Sand Particle Shape 6
2.4. Angle of Repose Test 7
2.5. Continuum Approach vs. Discrete Element Modeling 8
3. PREPERATION OF SAMPLES 10
3.1. Classification of Soils 10
3.1.1. Classification of Soils According to Particle Size 10
3.1.2. Classification of Sands and Gravels 11
3.1.2.1. Uniformly Graded Soils 11
3.1.2.1. Well - Graded Soils 12
3.1.2.1. Poorly - Graded Soils 13
3.2. Selection of Materials 13
3.3. Preparation of Samples 15
3.4. Sieve Analysis 17
3.4.1. Equipment Used in Sieve Analysis 17
3.4.2. Testing Procedure 19
3.5. Determination of Specific Gravity 20
3.6. Laboratory Procedure for Specific Gravity Determination 21
3.6.1. Equipments Used 21
3.6.2. Test Procedure 22

3.6.3. Computation 23
4. DETERMINATION OF SHAPE PARAMETERS OF GRAINS 24
4.1. The Law of Large Numbers 29
5. ANGLE OF REPOSE 33
5.1. Definition of Angle of Repose 33
5.2. Experimental Method of Obtaining Angle of Repose 34
5.3. Results of Angle of Repose Experiments 40
6. DISTINCT ELEMENT MODELING USING PFC2D 42
6.1. The Distinct Element Method 43
6.2. The PFC2D Particle Flow Model 44
6.3. Force Displacement Law 47
6.4. Law of Motion 52
6.5. Limitations of Two-Dimensional Modeling 55
6.5.1. Stress and Strain 55
6.5.2. Packing and Porosity 56
6.5.3. Mass Properties 57
7. TWO DIMENSIONAL MODELLING OF ANGLE OF REPOSE EXPERIMENT 58
7.1. Simple Idealized Model Consisting of Balls with Different Friction Coefficient 59
7.2. Utilization of Clumps to Reflect Particle Shape 60
7.3. Effect of Clump Detail on Angle of Repose Value 62
7.4. Modeling of Different Sand Specimens Using Clumps Containing Four Balls 66
8. RESULTS AND DISCUSSION 71
9. CONCLUSION 75
REFERENCES 77

LIST OF FIGURES

Figure 3.1. Examples of grain size distribution curves for sands and gravels 12

Figure 3.2. Samples of different sands 14

Figure 3.3. Washing of grains smaller than No. 200 sieve 15

Figure 3.4. Owen drying of samples 16

Figure 3.5. Sieving of sand samples 16

Figure 3.6. Separated sand specimens from sieve analysis 17

Figure 3.7. Stack of sieves and sieve shaker 18

Figure 3.8. Specific gravity experiment setup 22

Figure 4.1. Particle shape determination chart 24

Figure 4.2. A sample of calculation of shape parameters 25

Figure 4.3. Samples of stereomicroscope photographs on shape determination chart .. 27

Figure 4.4. The long term behavior of the relative frequency of two heads in many tosses of four coins 30

Figure 4.5. The long term behavior of the mean outcome of many trials 32

Figure 5.1. Angle of repose 33

Figure 5.2. Formation of slope 34

Figure 5.3. Device for measuring the angle of repose ϕ_{rep} : pedestal with depression, ring and spacer 35

Figure 5.4. Device for measuring the angle of repose ϕ_{rep} : plate with scaled poles 36

Figure 5.5. Apparatus for determining sand repose angle 36

Figure 5.6. The funnel used in experiment 37

Figure 5.7. The frame used in angle of repose experiment 38

Figure 5.8. Pouring of the sand 38
Figure 5.9. Flow of sand 39
Figure 5.10. Side view of the pile formed 39
Figure 5.11. Top view of the pile formed 39
Figure 5.12. Measurement technique of the angle of repose 40
Figure 6.1. Notation used to describe ball-ball contact 48
Figure 6.2. Notation used to describe ball-wall contact 48
Figure 6.3. Determination of normal direction for ball-wall contact 49
Figure 7.1. Observed pile for $\mu = 0.6$ 59
Figure 7.2. Observed pile for $\mu = 0.9$ 60
Figure 7.3. Making clumps from the chart that reflect the shape of grain 61
Figure 7.4. Shapes of clumps selected for different types of sands 63
Figure 7.5. Clump consists of two balls 64
Figure 7.6. Two different clumps consist of two identical balls 64
Figure 7.7. Results of numerical angle of repose test on different clumps 65
Figure 7.8. Obtaining angle of repose value from numerical experiment 67
Figure 7.9. Angle of repose vs. interparticle friction coefficient for uniformly graded sands 68
Figure 7.10. Angle of repose vs. interparticle friction coefficient for well-graded sands 69
Figure 8.1. Change in angle of repose values with interparticle friction coefficient for uniformly graded sand 72
Figure 8.2. Angle of repose values for different interparticle friction coefficient for well graded sands 73

LIST OF TABLES

Table 3.1. Particle Size Classifications 10

Table 3.2. Stack of sieves used 16

Table 3.3. U.S. Standard Sieve Sizes 18

Table 3.4. Specific Gravity values of five sand specimens 21

Table 4.1. Average values of shape parameters for grains between No.10 and No.16 sieves 26

Table 4.2. Average values of shape parameters for grains between No.16 and No.40 sieves 26

Table 4.3. Average values of shape parameters for grains between No.40 and No. 70 sieves 26

Table 4.4. The result of first 6 trials of the toss of four coins 30

Table 4.5. The mean $\bar{x}$ of all observations to date after each of the first few trials 31

Table 5.1. Angle of repose values obtained from experiments 41

Table 7.1. Radius, x and y coordinates of clumps 62

Table 7.2. Values obtained from uniformly graded sand specimens 68

Table 7.3. Values obtained from well-graded sand specimens 69

Table 8.1. Results of angle of repose experiment 71

Table 8.2. Interparticle friction coefficients giving the same results as experiments for uniformly graded sands 72

Table 8.3. Interparticle friction coefficients giving the same results as experiments for well graded sands 73

LIST OF SYMBOLS / ABBREVIATIONS

C_u	Coefficient of uniformity
C_c	Coefficient of curvature
d	Distance
D_i	Grain size corresponding to i % fines
F_i	Contact force vector
G	Shear modulus
g_i	Body force acceleration vector
G_s	Specific gravity of soil solids
k	Tangent stiffness modulus at contact
K	Secant stiffness modulus at contact
m	Mass
M_i	Contact moment vector
n	Porosity
n_i	Unit normal vector
p_i	Probability of variable i
R	Radius
R	Roundness
S	Sphericity
t	Time
U^n	Overlap in normal direction
V	Velocity
W_{fs}	Weight of the flask filled with soil and water
W_{fw}	Weight of the flask filled with de-aired water only
W_s	Weight of dry soil
$\dot{x}$	Translational velocity
$\ddot{x}$	Translational acceleration
x_i	Position vector

μ	Friction coefficient
μ_i	Mean of a variable *i*
ν	Poisson's ratio
σ_i	Standard deviation of variable *i*
ϕ_{rep}	Angle of repose
ω	Rotational velocity
$\dot{\omega}$	Rotational acceleration

ASTM	American Society for Testing and Materials
DEM	Distinct element method
PFC2D	Particle Flow Code in two dimensions

1. INTRODUCTION

In all standard soil mechanics laboratory experiments the granular materials like sands and gravels are examined at macro-scale. Even the smallest sized samples that are used in soil element testing contain numerous grains that are in contact. The underlying assumption here is that the behavior of the soil element tested reflects the behavior of the corresponding soil layer in the field. This approach clearly assumes in a simplistic sense a continuum behavior for multiphase granular materials. However, the observed macro-scale behaviors of granular materials are dependent on the micro properties of individual grains forming the bulk material. The granular materials that are used in soil mechanics laboratory experiments, such as gravels and sands are treated as a continuous media. However, in classical soil mechanics practicality dictates that grain-to-grain interactions are ignored. Though with the advance of computers, for geotechnical engineers it is becoming feasible to consider these intergranular interactions.

Within the context of continuum mechanics approach the interactions of grains are not considered, therefore the discontinuous nature of sands and gravels can not be represented. Discrete element method, which was first extended to soil mechanics using two dimensional disk elements and three dimensional spheres by Cundall and Stack (1979), is known to be an effective method for describing the particle interactions within an assembly basically using Newton's second law motion and force displacement law. The distinct element method has the following features (Mustoe and Miyata, 2001). Firstly, an automatic contact detection algorithm involving a series of sorting actions and geometry checks of increasing complexity. Secondly, a contact force generation algorithm that can either compute total force or incremental force updates. Thirdly, a time integration procedure which is explicit involving a two step generalized velocity and position update. The distinct element method has been used primarily to study the fabric and structure of granular media during loading and to aid in development of constitutive relations for soil using disks and spheres (Bathurst et al. 1988, Zhang and Cundall 1986, Oner 1984).

In two-dimensional distinct element method, the particles are defined using balls which are either treated as disks or spheres. Representation of different particle shapes is

possible by creating clumps that are formed by attaching several balls together. There is no limitation for the number of balls used to generate a single clump representing a single grain, except computational time. Increasing the number of balls used in a single clump provides a better representation of grain shape, but causes significant increase in runtime of the model.

There are two contact models that are readily defined in PFC2D, namely linear contact model and Hertz contact model. The Hertz model, which is used in this study, provides sliding behavior and stiffness that varies as a function of elastic constants of the two contacting entities, overlap and normal force. It is strictly applicable only to the case of spheres in contact. This is the main reason of selecting Hertz model, sphere representation is more appropriate for sand grains rather than disk elements. The model is defined by two parameters, namely shear modulus G and Poisson's ratio ν of two contacting balls.

The behavior of the granular materials under shear is dependent on the properties of individual grains that are interacting with each other. Distinct element method considers these interactions and the governing laws are defined for the contacts of these individual grains. Therefore computer simulations of the soil mechanics laboratory experiments using distinct element programs such as PFC2D will give a better understanding of phenomena at particle level. The summation of all the effects at particle contact level produces the response of the entire assembly.

Particle size is generally taken as a criterion to classify soils. Soil particles are classified as gravel, sand, silt, or clay according to particle size. Sieve analysis and hydrometer tests are done to obtain particle size distribution curves to classify soils according to the relative proportions of different sized grains. In addition to the particle size, there are other factors that influence the continuum behavior of soils. For example, the shapes of the particles also affect the packing, porosity, and shear strength of granular soils. The variation of shapes of individual grains in a bulk material of sand consisting of granules is random and involves great deal of ambiguity.

The micro properties of granules can be identified in two scales; surface texture and surface shape. Surface texture is expressed by roughness of the grain and surface shape is expressed by roundness and sphericity. Parameters of surface shape can be identified by taking photographs. There are classifications for the surface shape depending on the geometrical properties of grains. Besides this, surface roughness is an unknown parameter at micro-scale. The coefficient of friction between interacting particles is mainly caused by the roughness of the grains. The roughness of the sand grains that are used in soil mechanics experiments are not known, therefore the value of intergranular friction coefficient is a missing parameter in the model.

The goal of this study is to develop a suitable method that would yield the representative value of coefficient of friction that can be used in distinct element modeling of sand particles' interactions. The method used in this study is discrete element modeling of angle of repose tests which are conducted in the laboratory. In the numerical models the coefficient of friction value is varied until the angle of repose in the DEM model matches the physical one. For this purpose dry sand specimens are used.

There are various shear strength tests that are used in soil mechanics. Angle of repose test is one of them, which has some important advantages over the other tests, considering the numerical modeling of the test conditions. In most of soil mechanics laboratory shear strength tests such as triaxial test or direct shear test, the soil sample is confined in a geometrically defined space, therefore porosity or relative density of the material affects the results significantly. It is possible to achieve desired porosity of the assembly when using balls to represent grains, but if particle shape is also included in the model with using clumps, it is not possible to obtain the desired porosity. Besides, there is no clear relationship between 2D porosity and 3D porosity. This is a major handicap. Angle of repose test gives the shear strength value in the loosest state of soil. No external loads are applied to soil sample, soil grains freely fall from a specified height with gravitational loading. Therefore, there is no need to generate the initial assembly with any specified porosity. Only gravitational load is applied to the clumps oriented randomly at the initial stage. Porosity is not an initial condition for angle of repose test. Another advantage of angle of repose test is that number of grains used in the model is less important compared to other shear strength laboratory tests. Size effect is more critical

when modeling triaxial or direct shear test. Therefore, these properties of the angle of repose test simplify the definition of the numerical model and eliminate the inconsistencies with the real situation.

The selected testing material is sand. To test samples having different shape properties, one crushed sand sample, two sea sand samples, and two river sand samples are used in the laboratory tests. The underlying cause for this decision is the desire to observe the behavior of different shaped sand samples.

Shape varies with particle size, particularly in crushed sands: smaller particles are more planar and have sharper corners (Cho et al., 2006). Shape dispersion in this study is minimized by determining the shape parameters for grains remaining between different sieve openings. Firstly, uniformly graded sand samples are tested. Afterwards, well graded sand samples were also analyzed. Well-graded samples were obtained by mixing the soils remaining between different sieves. Roundness and sphericity values are determined using the particle shape determination chart of Cho et al. (2006). The shape parameter values are determined to model the grains in distinct element program. The grading of the specimens is also modeled by giving various radii values to the balls used in clumps.

The intergranular coefficient of friction is evaluated in this study, using distinct element modeling of angle of repose test. In the second chapter, previous related studies are summarized as literature survey. In the third chapter, selection of materials and preparation of these materials for the angle of repose test is explained. In the fourth chapter, determination of shape parameters of the grains is discussed. The fifth chapter explains the angle of repose test. The sixth chapter is about two dimensional modeling using distinct element program PFC2D. In the seventh chapter, the 2D model constructed for the angle of repose test is explained. In the eighth chapter, the results are discussed after which the conclusions are given.

2. LITERATURE REVIEW

2.1. Introduction

Sand is a granular material composed of individual particles. The behavior of sand under shear has been investigated by many researchers for years. In soil mechanics, either laboratory or field testing is used to define the properties of soils. In these tests the behavior is investigated at macro-scale, therefore continuum mechanics approach is valid. However, properties of individual grains, and grain to grain interactions are ignored in continuum mechanics point of view. In recent years, with the development of computer technology, numerical simulations of these test become available for researchers to investigate the particulate behavior of soils at micro scale. Distinct element method is a powerful tool that is most widely used to analyze soil behavior with using discrete particles. Surface roughness which is a measure of intergranular coefficient of friction is an important parameter for numerical models. The effect of intergranular friction coefficient on shear strength is a line of research still in progress.

This chapter presents an overview of the current work on the engineering behavior and strength of sands, the effect of particle shape on strength properties, and the angle of repose test.

2.2. Engineering Behavior and Strength of Dry Sand

Various factors that determine the shear resistance of dry granular soil fall into two general groups. The first group includes those factors that affect the shear resistance of a given soil: the void ratio of the soil, the confining stresses, the rate of loading, etc. It is necessary to understand the influence of these factors so that the strength appropriate for a practical problem can be calculated. Of these factors, void ratio and confining stress are by far the most important. The second group indicates those factors that cause the strength of one soil to differ from the strength of another soil, even for the same confining stress and

void ratio: the size, shape, and gradation of the particles making up the soil (Lambe and Whitman, 1969).

Relative sliding between particles is the most important mechanism of deformation within a soil mass. Hence the resistance of soil to deformation is influenced strongly by shear resistance at contacts between particles. It is emphasized that the shear resistance between mineral surfaces is only part of the resistance of a soil mass to shear or compression. Also very important is interlocking of particles, which is largely a function of packing density. (Lambe and Whitman, 1969).

The shear behavior of sand is different for loose and dense conditions. In dense sand there is a considerable degree of interlocking between particles. Before shear failure can take place, this interlocking must be overcome in addition to the frictional resistance at the points of contact. In general, the degree of interlocking is greatest in the case of very dense, well-graded sands consisting of angular particles. The term dilatancy is used to describe the increase in volume of a dense sand during shearing. In the case of initially loose sand there is no significant particle interlocking to be overcome and the shear stress increases gradually to an ultimate value without a prior peak, accompanied by a decrease in volume (Craig, 2004).

2.3. Sand Particle Shape

Cho et al. (2006) presented their experimental data and results from published studies into two databases to explore the effects of particle shape on packing density and on the small-to-large strain mechanical properties of sandy soils. It is stated that the direct measurement of roughness is cumbersome: the fractal nature of rough surfaces implies that there is no characteristic scale on the surface itself. Therefore, the relevant “observation length scale” for roughness is the interparticle contact area. Shape parameters can be inferred from macroscale behavior of the soil mass. For instance, particle shape affects granular flow on inclined planes, residence time on sieves, and sedimentation time in a fluid column. However, it is not possible to separate the relative contributions of

roughness, sphericity, and roundness from such individual measurements (Cho et al., 2006).

The findings of Cho et al. shows that particle shape characteristics manifest at various scales: the global form at the scale of the particle, angularity at the scale of major surface features, and roughness at the scale of surface texture. Each scale reflects aspects of formation history, and participates in determining the global behavior of the soil mass. The decrease in particle regularity (decrease sphericity and/or roundness) leads to increase in extreme void ratios and void ratio interval (Cho et al., 2006).

Rouse et al. (2008) investigated the influence of roundness on the void ratio and strength of uniform sand. Uniformly graded coarse sand with no fines, called Badger sand is investigated. Three index properties, namely e_{min}, e_{max}, and roundness are measured. Relationships between extreme void ratios and roundness is found. Relationships are also given for angle of repose and constant volume friction angle values versus roundness. The effect of roundness is significant in this study and it is recommended to report roundness values in experimental studies (Rouse et al., 2008).

Santamarina and Cascante (1998) investigated the effect of surface characteristics on soil behavior, and they report experimental results on the role of surface roughness on wave propagation parameters. It has been found that, while small-strain stiffness decreases with surface roughness, large-strain stiffness and the angle of shear resistance increase with surface roughness (Santamarina and Cascante, 1998).

2.4. Angle of Repose Test

Carrigy (1970) measured angle of repose of several materials like metal cubes and spheres, glass beads, and crushed sand in air and under water. He stated that, although the angle of repose appears in a number of empirical engineering equations relating to the transport of sand by moving water and the calculation of static earth pressures, no simple method of measuring this angle is available. In fact, no agreement has been reached as to what angle should be measured. Physicists and some engineers apply the term to the angle

of slope (with the horizontal) of an inclined plane at which a body resting on the plane will begin to slide. Most geologists and engineers, however, use the term to define the angle (with the horizontal) at which loose granular material will stand when piled or dumped. He concluded that shape and surface characteristics of the particles have the greatest effect on the angle of repose (Carrigy M. A., 1970).

Pohlman et al. (2006) have investigated the effect of nanoscale variations in the surface roughness of individual particles on macroscale granular flow characteristics. Experiments were conducted in circular rotating tumblers with smooth and rough 2 and 3 mm steel particles. The dynamic angle of repose for rough particles increased by 10° to 25° over that of smooth particles over a wide range of rotation speeds. For mixtures of smooth and rough particles, the angle of repose increased monotonically with increasing concentration of rough particles (Pohlman et al., 2006).

2.5. Continuum Approach vs. Discrete Element Modeling

In the study of Ting et al. (1989), two dimensional disk based implementation of the distinct element method is validated using numerical simulations of standard geotechnical laboratory tests, such as one-dimensional compression, direct simple shear, and triaxial tests. These test results indicate that the two dimensional DEM can simulate realistic nonlinear, stress history-dependent soil behavior appropriately when individual particle rotation is inhibited. It is stated that, it is not possible to specify desired aggregate soil properties at the outset such as Young's modulus, Poisson's ratio, Mohr-Coulomb cohesion intercept, and angle of internal friction. Instead, it is necessary to choose appropriate normal and tangential spring stiffnesses and damping, contact strength parameters for both disk-disk and disk-wall interfaces, as well as material size, specific gravity and gradation. Many of these contact properties may be computed from physical properties (Ting et al., 1989).

Zhou et al. (2001) made a numerical study of the angle of repose, by means of a modified distinct element method. Emphasis is given to the effect of variables related to the factors such as particle characteristics, material properties, and geometrical constraints.

The results show that sliding and rolling frictions are primary reasons for the formation of a sand pile; particle size and container thickness significantly influence the angle of repose; and the angle of repose is not so sensitive to density, Poisson's ratio, damping coefficient, and Young's modulus. Increasing rolling friction coefficient or sliding friction coefficient increases the angle of repose. Conversely, increasing particle size or container thickness decreases the angle of repose (Zhou et al., 2001).

Huang et al. (2008) investigated granular material behavior by numerical approach with the aid of distinct element method. Different from experimental approach, the numerical method has advantages of providing the mechanical behaviors of granular assembly in both the macro and micro scales. They conduct a series of biaxial compression tests on the samples with different initial confining pressures and initial densities, under both the constant volume and drained conditions. It is concluded that, DEM successfully simulates the typical granular material behavior in biaxial compression mode (Huang et al., 2008).

3. PREPERATION OF SAMPLES

3.1. Classification of Soils

3.1.1. Classification of Soils According to Particle Size

In the general sense of engineering, soil is defined as the uncemented aggregate of mineral grains and decayed organic matter (solid particles) along with liquid and gas that occupy the empty spaces between the solid particles (Das, 2007). Civil engineering, especially geotechnical engineering is interested in the properties such as its origin, grain-size distribution, ability to drain water, compressibility, shear strength, and so on. The collection of minerals constitutes the solid phase of the soil that forms the soil aggregates that are the product of rock weathering. Many of the physical properties of soil are reasoned by size, shape, and chemical composition of the grains.

Table 3.1. Particle Size Classifications (ASTM, 2005)

	Grain Size (mm)			
Name of Organization	**Gravel**	**Sand**	**Silt**	**Clay**
U.S. Department of Aggriculture (USDA)	>2	2 to 0.05	0.05 to 0.002	<0.002
American Association of State Highway and Transportation Officials (AASHTO)	76.2 to 2	2 to 0.075	0.075 to 0.002	<0.002
Unified Soil Classification System (U.S. Army Corps of Engineeers, U.S. Bureau of Reclamation, and American Society for Testing and Materials)	76.2 to 4.75	4.75 to 0.075	Fines (i.e., silts and clays)<0.075	

Table 3.1 shows the particle size classifications developed by the U.S. Department of Agriculture, the American Association of State Highway and Transportation Officials, and the U.S. Army Corps of Engineers and U.S. Bureau of Reclamation. The Unified Soil Classification System is now almost universally accepted and has been adopted by the American Society for Testing and Materials (ASTM).

Gravels are pieces of rocks with occasional particles of quartz, feldspar, and other minerals. Sand particles are made of mostly quartz and feldspar. Other mineral grains also may be present at times. Silts are the microscopic soil fractions that consist of very fine quartz grains and some flake-shaped particles that are fragments of micaceous minerals. Clays are mostly flake-shaped microscopic and submicroscopic particles of mica, clay minerals, and other minerals.

3.1.2. Classification of Sands and Gravels

Grain size distribution curves enable sand and gravels to be classified in three main types: uniform, well graded, and poorly graded.

3.1.2.1. Uniformly Graded Soils: In uniform soils, the majority of grains are nearly the same size. The grading curve is very steep, as shown by curve A in Figure 3.1, which represents a uniform sand. The uniformity in soils is characterized by the uniformity coefficient C_u.

$$C_u = \frac{D_{60}}{D_{10}} \tag{2.1}$$

where D_{10} is the grain size corresponding to 10% finer and D_{60} is the grain size corresponding to 60% finer. C_u represents the average slope of the grain size distribution between 10 and 60%. The smallest possible value for C_u is equal to 1 and corresponds to a perfectly uniform assemblage of grains of identical size.

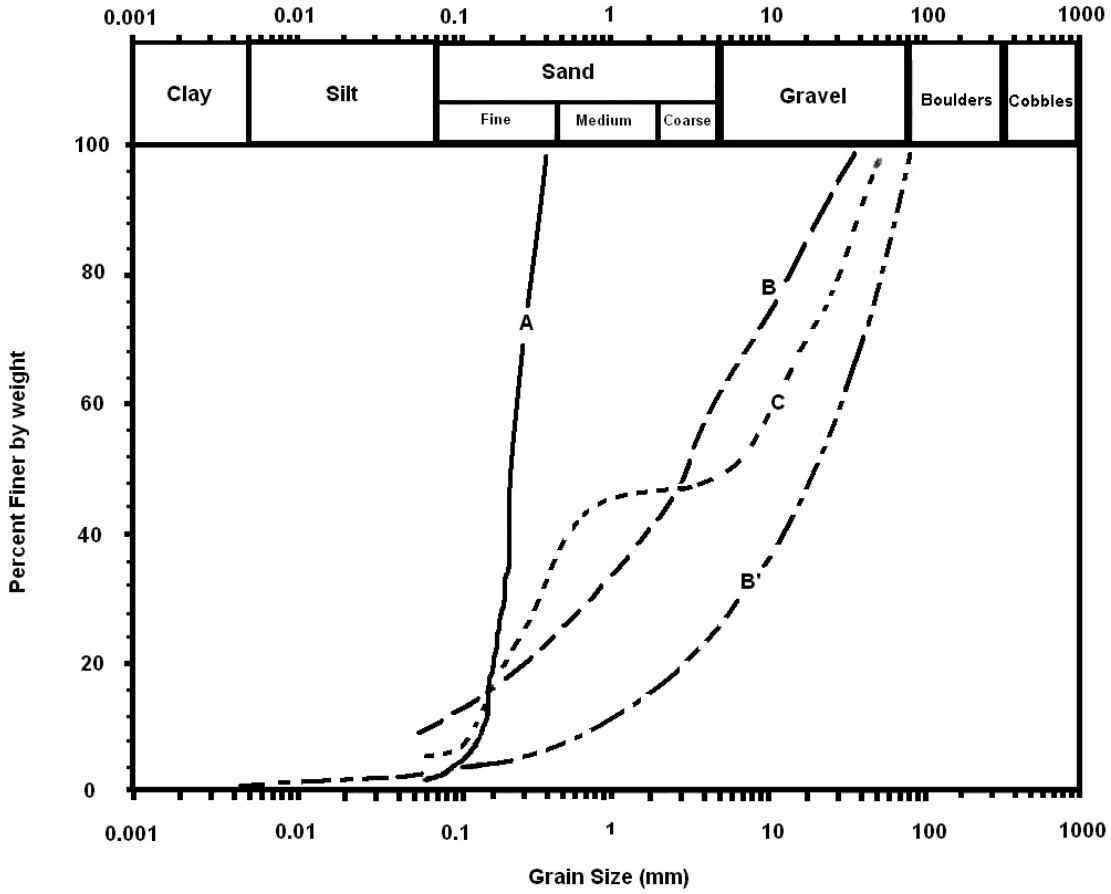


Figure 3.1. Examples of grain size distribution curves for sands and gravels (Head, 1984)

3.1.2.2. Well-Graded Soils: Well-graded soils contain a wide and even distribution of particle sizes. A well-graded silty sand and gravel is shown by curve B in Figure 3.1. The smooth concave upward-grading curve is typical of well-graded material. Particle size distribution can be characterized by its curvature, and more specifically by the coefficient of curvature C_c:

$$C_c = \frac{D_{30}^2}{D_{10} D_{60}} \tag{2.2}$$

where D_{30} is the grain size corresponding to 30% finer. By definition, gravels are considered to be well graded when $C_u > 4$ and $1 < C_c < 3$. Sands are considered to be well graded when $C_u > 6$ and $1 < C_c < 3$.

3.1.2.3. Poorly-Graded Soils: The term poorly graded applies to any soil, including uniform soil, which does not comply with the description of well graded. Poorly graded soils are deficient in certain sizes. Gap-graded materials are examples of poorly graded materials with missing ranges of particle sizes. For example, curve C in Figure 3.1 has a flat part indicating that there are only a few particles in the range 1 to 10 mm. In practice, gap-graded materials are generally found in the coarse sand, fine gravel range.

3.2. Selection of Materials

For evaluating the effect of grain shape on the global friction angle for granular materials, five different sand specimens are selected for the experiments, which differ according to their shapes. For this purpose, two river sands, two seashore sands, and one crushed sand are selected. Previous studies on grain shape (Margolis and Krinsley, 1974; Rahaman, 1995) conclude that particle size and shape reflect material composition, grain formation, and release from the mineral matrix, transportation, and depositional environments. Mechanical and chemical processes determine grains shape once it is released from the matrix. The mechanical processes are stronger in rivers compared to seas. Therefore river sands are more regular in shape than seashore sands, and the crushed sands are angular and platy.

A general appearance of the different sand specimens can be seen in Figure 3.2. Grain shape can not be detected in this figure but microscopic photographs of the grains are also taken and these can be found in Section 4.

Figure 3.2 gives an idea about how the texture and shapes of the grains change from sample to sample. These five different types of sands are:

1. Sile Sand (sea sand)
2. Crushed Sand (crushed stone)
3. Sakarya River Sand
4. Silivri Sand (sea sand)
5. Meric River Sand

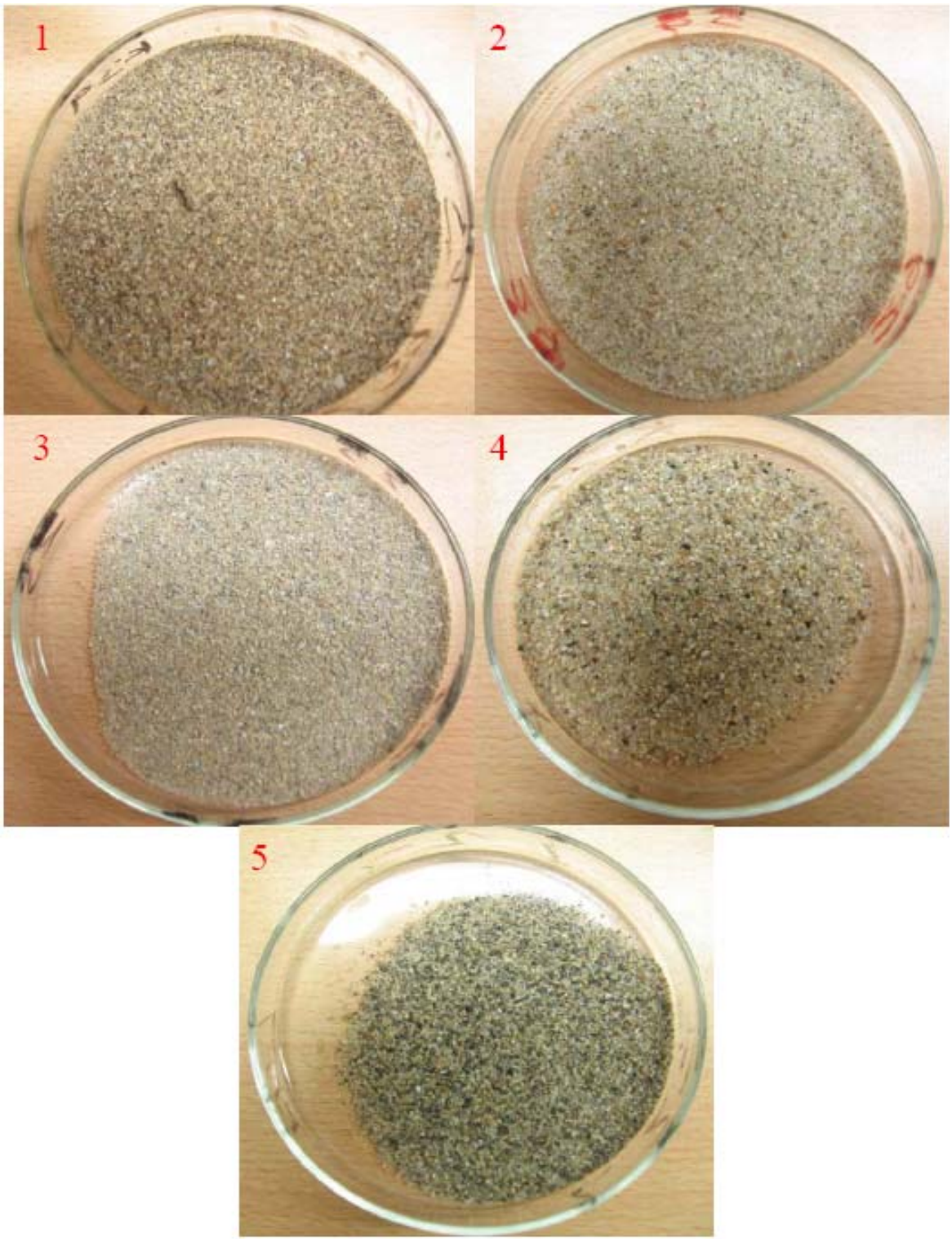


Figure 3.2. Samples of different sands

(1.Sile Sand, 2.Crushed Sand, 3.Sakarya Sand, 4.Silivri Sand, 5.Meric Sand)

3.3. Preparation of Samples

The samples are prepared by wet sieving of the specimens. ASTM D2217, Standard Practice for Wet Preparation of Soil Samples for Particle Size Analysis and Determination of Soil Constants is followed during the conduction of the test. First, the sands are washed using a bottom pan and No. 200 (0.075 mm) sieve to get rid of small portion of particles sized as silts and clays (Figure 3.3). Then wet samples are oven dried (Figure 3.4). Then oven dried samples are separated according to particle size using a sieve shaker (Figure 3.5). The stack of sieves used is summarized in Table 3.2. The soil remaining on top of each sieve is collected into plastic bags (Figure 3.6). For the ease of modeling in discrete element modeling code and for the purposes of comparison, sand particles are retained between the sieves No. 16 and No. 40 are used in the tests. The same size range for sand samples is also used for specific gravity determination and stereomicroscope views. Therefore, all of the experiments are made with uniform sand samples and accordingly, the sand have particle radii between 1.18 mm and 0.425 mm. The radius of the spheres in the PFC2D model is also uniformly distributed between these values.



Figure 3.3. Washing of grains smaller than No. 200 sieve



Figure 3.4. Owen drying of samples



Figure 3.5. Sieving of sand samples

Table 3.2. Stack of sieves used

Sieve No.	Opening Size (mm)
No. 4	4.75
No. 10	2.00
No. 16	1.18
No. 40	0.425
No. 70	0.212
No. 100	0.150
No. 200	0.075



Figure 3.6. Separated sand specimens from sieve analysis

3.4. Sieve Analysis

The sieve analysis determines the grain size distribution curve of soil samples by passing them through a stack of sieves of decreasing mesh opening sizes and by measuring the weight retained on each sieve. The sieve analysis is generally applied to the soil fraction larger than 75 μm. Grains smaller than 75 μm are sorted by using sedimentation (e.g., hydrometer or pipette analysis). Sieving can be performed in either wet or dry conditions. Dry sieving is used only for soils with a negligible amount of plastic fines, such as gravels and clean sands, whereas wet sieving is applied to soils with plastic fines.

3.4.1. Equipment Used in Sieve Analysis

The equipment used in sieve analysis includes:

- Series of standard sieves with openings ranging from 7.5 cm to 75 μm, including a cover plate and bottom pan. Figure 3.7 shows an example of a stack of sieves. Sieves are generally constructed of wire screens with square openings of standard size. Table 3.3 lists the number and mesh opening sizes of the U.S. standard sieves. Only a few sieves in Table 3.3 are selected for the sieve analysis. The total number and mesh sizes of the sieves are selected to cover the range of grain sizes in an even distribution on a logarithmic scale.

- Sieve shake.
- Balances sensitive to 0.1 g.
- Soft wire brush.
- Sample splitter or riffle for dividing large soil samples into smaller samples with identical grain size distribution.
- Mortar and rubber-covered pestle, for breaking up aggregations of soil particles.



Figure 3.7. Stack of sieves and sieve shaker

Table 3.3. U.S. Standard Sieve Sizes (ASTM E11,2009)

Sieve number	Sieve opening (mm)	Sieve number	Sieve opening (mm)
4	4.75	50	0.3
5	4	60	0.25
6	3.35	70	0.212
7	2.8	80	0.18
8	2.36	100	0.15
10	2	120	0.125
12	1.7	140	0.106
14	1.4	170	0.09
16	1.18	200	0.075
18	1	230	0.063
20	0.85	270	0.053
25	0.71	325	0.045
30	0.6	400	0.038
35	0.5	450	0.032
40	0.425	500	0.025
45	0.355	635	0.02

3.4.2. Testing Procedure

There are two different procedures for dry and wet sievings. Wet sieving is used when the small particles aggregate and form hard lumps, or coat the coarser particles.

Dry Sieving (Bardet, 1997):

1. Oven dry the sample, allow it to cool, and measure its weight.
2. Select a stack of sieves suitable to the soil being tested. The choice of sieves usually depends on experience, judgment, and the intended applications of grain size analysis. A stack of six or seven sieves is generally sufficient for most soils and applications. The top sieve should have an opening slightly larger than the largest particles. Arrange the stack of sieves so that the largest mesh opening is at the top and the smallest is at the bottom.
3. Attach a pan at the bottom of the sieve stack. Pour the sample on the top sieve. Add a cover plate to avoid dust and loss of particles while shaking.
4. Place the stack of sieves in the mechanical shaker and shake for about 10 min or until additional shaking does not produce appreciable changes in the amounts of material retained in each sieve.
5. Remove the stack of sieves from the shaker. Beginning with the top sieve, transfer its contents to a piece of paper or a large recipient. Carefully empty the sieve without losing any material, and use a brush to remove grains stuck in its mesh opening. Measure the weight of soil retained in each sieve and note the corresponding sieve mesh opening and number.
6. Repeat step 5 for each sieve. As a preliminary check, the weights retained on all the sieves and the bottom pan are added, and their sum is compared to the initial sample weight. Both weights should be within about 1%. If the difference is greater than 1% too much material was lost and weighing and/or sieving should be repeated.

Wet Sieving (Bardet, 1997):

1. Weigh the dry specimen as for dry sieving.

2. If the sample contains plastic fines, which tend to form hard lumps or to coat the coarser particles, place the oven-dried sample in a pan filled with enough water to cover all the material and allow it to soak until all the soil lumps or coatings have disintegrated. Soaking may take 2 to 24 hours, depending on the soil.
3. Transfer the sample to a No. 200 sieve, or to a set of No. 4 to No. 200 sieves if the sample contains an appreciable amount of coarse particles. Do not overload the fragile No. 200 sieve. Wash the sample thoroughly through the sieves, discarding the material passing the No. 200 sieve. Larger particles may be individually washed and removed from the sieves.
4. Oven dry the retained material, and weigh it after it has cooled. Record the difference between the dry weights before and after washing.
5. Use the dry sample for dry, sieving starting at step 2.

3.5. Determination of Specific Gravity

The specific gravity G_s of a soil is the ratio between the unit masses of soil particles and water. G_s is useful for determining weight-volume relationships. In this study it becomes necessary to find specific gravity of the sands by experimental technique to be able to calculate porosity in triaxial tests and to give the density value to the balls and clumps which represent the solid phase of sands in the discrete element program PFC2D.

The specific gravity of soil solids is determined following the ASTM standard D854, Standard Test Methods for Specific Gravity of Soil Solids by Water Pycnometers. The procedure of the test is given in Section 3.6. The test method covers the determination of the specific gravity of soil solids that pass the 4.75 mm (No. 4) sieve, by means of water pycnometer. Method B procedure from ASTM D854 is appropriate for oven dried specimens; therefore it is used in this case. By definition, specific gravity of soil solids is defined as, the ratio of the mass of a unit volume of a soil solids to the mass of the same volume of gas-free distilled water at 20 °C (ASTM D854).

The specific gravity of soil solids is used in calculating the phase relationship parameters for soils, such as void ratio and degree of saturation. In this study, because the

density value of the balls used in distinct element method is important in shear behavior, the specific gravity is calculated precisely.

500 mL Labware pycnometers are used in the test. According to ASTM D854 recommended mass for test specimen when using 500 mL pycnometer is given as 100±10 g. 100 g of sand is used for the test. The lab temperature was 20°C, therefore no correction is made for temperature.

The values of specific gravity are summarized in Table 3.4.

Table 3.4. Specific Gravity values of five sand specimens

Soil	Specific Gravity
Sile Sand	2.63
Silivri Sand	2.69
Crushed Stone	2.84
Meric River Sand	2.58
Sakarya River Sand	2.68

3.6. Laboratory Procedure for Specific Gravity Determination

The laboratory book of Bardet (1997), Experimental Soil Mechanics is used as a main reference in this section.

3.6.1. Equipments Used

The equipment for determination of specific gravity includes:

- Volumetric flasks (250 or 500 mL) with stoppers numbered and calibrated. (Figure 3.8)
- Vacuum pump.
- Balance accurate to 0.01 g.
- Distilled deaired water.
- Thermometer, ranging from 0 to 50 °C accurate to 0.5 °C.

- Drying oven.
- Evaporating dish.



Figure 3.8. Specific gravity experiment setup

3.6.2. Test Procedure

1. Take a sample of 100 to 120 g of air-dried soil. For fine-grained soils, mix the sample with water in an evaporating dish to make about 200 ml. of soil-water mixture. For clays, transfer the soil-water mixture into a malt mixer container and mix it for about 5 to 10 mm. No soaking is required for sand and fine gravel. However, the aggregates should be broken into pieces small enough to go into the volumetric flask.
2. Transfer the soil-water mixture from the evaporating dish into the volumetric flask. Wash any remaining soil into the flask using a wash bottle. Add sufficient water to fill the flask two-thirds to three-fourths full. Do not fill it completely, because its contents must be agitated under vacuum.
3. Attach the flask to a vacuum line and for at least 10 min gently agitate the mixture while keeping it away from the flask stopper. The reduced air pressure should cause the water to boil.

4. When the de-airing process is complete, add deaired water to fill the calibrated flask volume.
5. Measure the weight of the flask. Measure the water temperature, which should be close to that of the temperature of flask calibration.
6. Empty the flask and its contents into a deep evaporating dish and oven dry. Measure the weight of dry soil.
7. Repeat the test to calculate additional values of G_s until the values of G_s are within 2% of each other.

3.6.3. Computation

The specific gravity G_s of a soil is calculated as follows:

$$G_s = \frac{W_s}{W_s + W_{fw} - W_{fs}} \tag{2.3}$$

where W_s is the weight of the dry soil, W_{fs} the weight of the flask filled with soil and water, and W_{fw} the weight of the flask filled with de-aired water only.

4. DETERMINATION OF SHAPE PARAMETERS OF GRAINS

There are three important scales in particle shape. Definitions and their conventional evaluation in the form of dimensionless parameters follow (Figure 4.1) (Wadell 1932; Krumbein 1941; Powers 1953; Krumbein and Sloss 1963; Barrett 1980):

1. Sphericity S (eccentricity or platiness) refers to the global form of the particle and reflects the similarity between the particle's length, height, and width. Sphericity can be quantified as the diameter of the largest inscribed sphere relative to the diameter of the smallest circumscribed sphere.
2. Roundness R (angularity) describes the scale of major surface features which are typically one order of magnitude smaller than the particle size. Roundness is quantified as the average radius of curvature of surface features relative to the radius of the maximum sphere that can be inscribed in the particle.
3. Smoothness (roughness). Roughness describes the particle surface texture relative to the radius of particle. (Cho et. al., 2006)

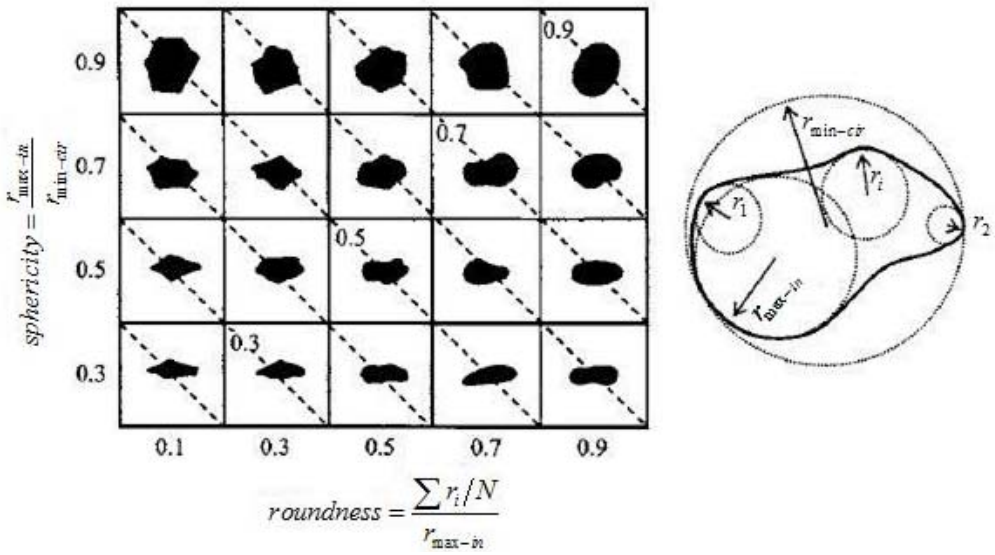


Figure 4.1. Particle shape determination chart (Cho et. al., 2006)

According to Cho et al., shape varies with particle size, particularly in crushed sands. Smaller particles are more planar and have sharp corners (Cho et al., 2006). By the

help of a stereomicroscope, pictures of individual grains are taken from five different sands for three different sieve gaps. Shape dispersion is minimized in this study by placing emphasis on specimen's uniformity. Based on previous studies (Rouse et. al., 2008) and the probability theorem "law of large numbers" the average of a sample approaches the mean of the population as the sample size increases (Moore and McCabe, 2003). In Section 4.1 brief description of the theory of law of large numbers can be found. Applying it to a sample size equal to 30 or more, roundness, sphericity, and regularity values are calculated using chart shown in Figure 4.1, and fitting 30 random grains (Figure 4.2 show an example of a grain fitted on the chart).

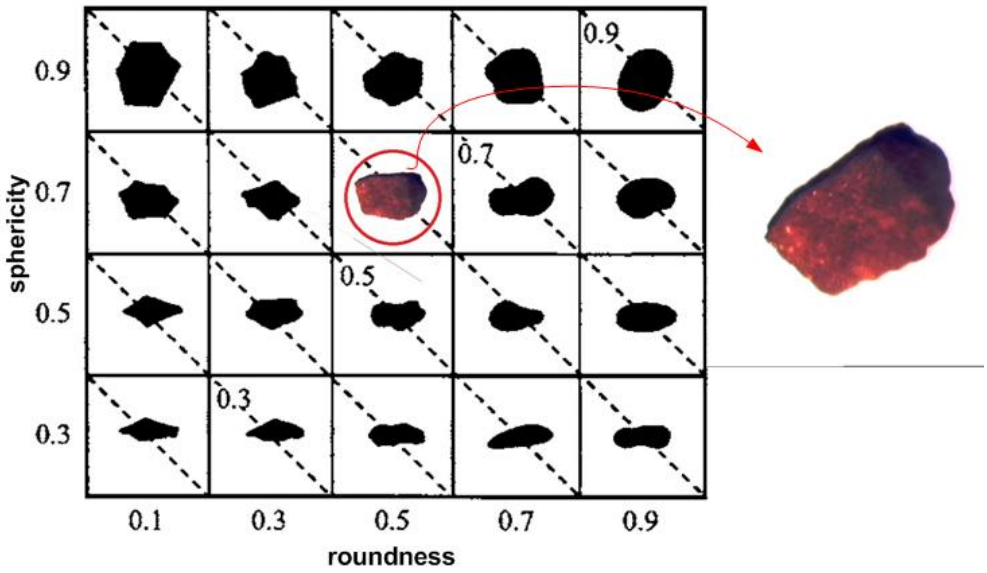


Figure 4.2. A sample of calculation of shape parameters

The mean values of roundness, sphericity, and regularity are tabulated in Table 4.1 to 4.3. These parameters are important because the behavior of particulate materials is directly affected by their fabric, the imposed state of stress and the inherent characteristics of particles, for example mineralogy, size, material strength and stiffness, angularity and surface characteristics (Santamarina, 1998).

Table 4.1. Average values of shape parameters for grains between No.10 and No.16 sieves

Sand Type	Roundness	Sphericity	Regularity
Sile Sand	—	—	—
Silivri Sand	0.58	0.72	0.65
Crushed Sand	0.39	0.71	0.55
Meric River Sand	0.53	0.75	0.64
Sakarya River Sand	0.51	0.71	0.61

Table 4.2. Average values of shape parameters for grains between No.16 and No.40 sieves

Sand Type	Roundness	Sphericity	Regularity
Sile Sand	0.46	0.65	0.56
Silivri Sand	0.41	0.76	0.58
Crushed Sand	0.39	0.62	0.51
Meric River Sand	0.54	0.78	0.66
Sakarya River Sand	0.58	0.76	0.67

Table 4.3. Average values of shape parameters for grains between No.40 and No. 70 sieves

Sand Type	Roundness	Sphericity	Regularity
Sile Sand	0.54	0.69	0.62
Silivri Sand	0.43	0.7	0.57
Crushed Sand	0.43	0.68	0.56
Meric River Sand	0.41	0.69	0.55
Sakarya River Sand	0.45	0.76	0.61

The roundness, sphericity, and regularity values of Sile sand for sieves between No. 10 and No. 16 is missing because in that gap no samples can be obtained for this particular sand. More examples of the grain photos attached on particle shape determination chart like the sample in Figure 4.2 can be found in coming two pages in Figure 4.3. These values are used in creation of clumps that will be explained in Section 7.2.

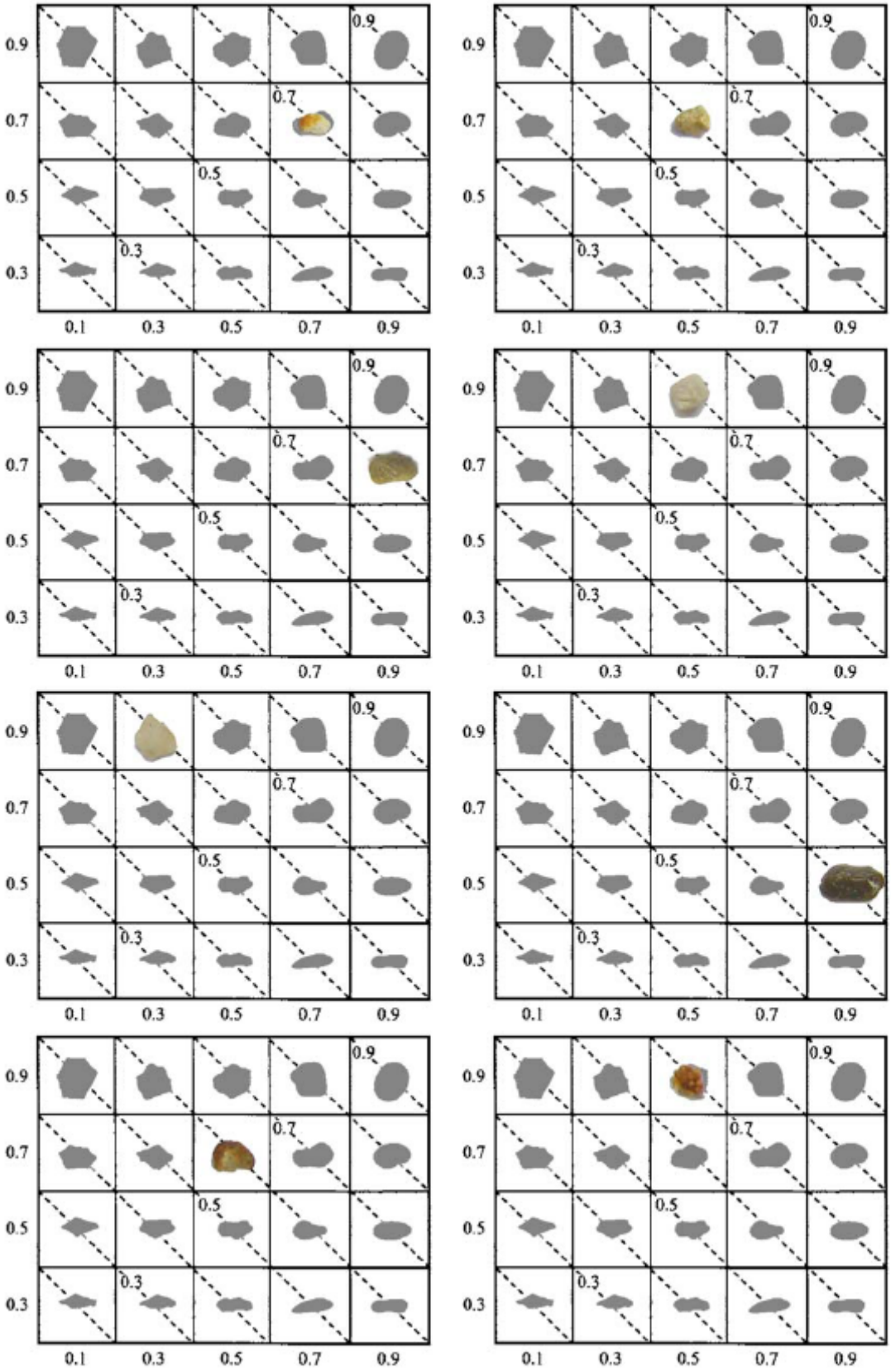


Figure 4.3. Samples of stereomicroscope photographs on shape determination chart

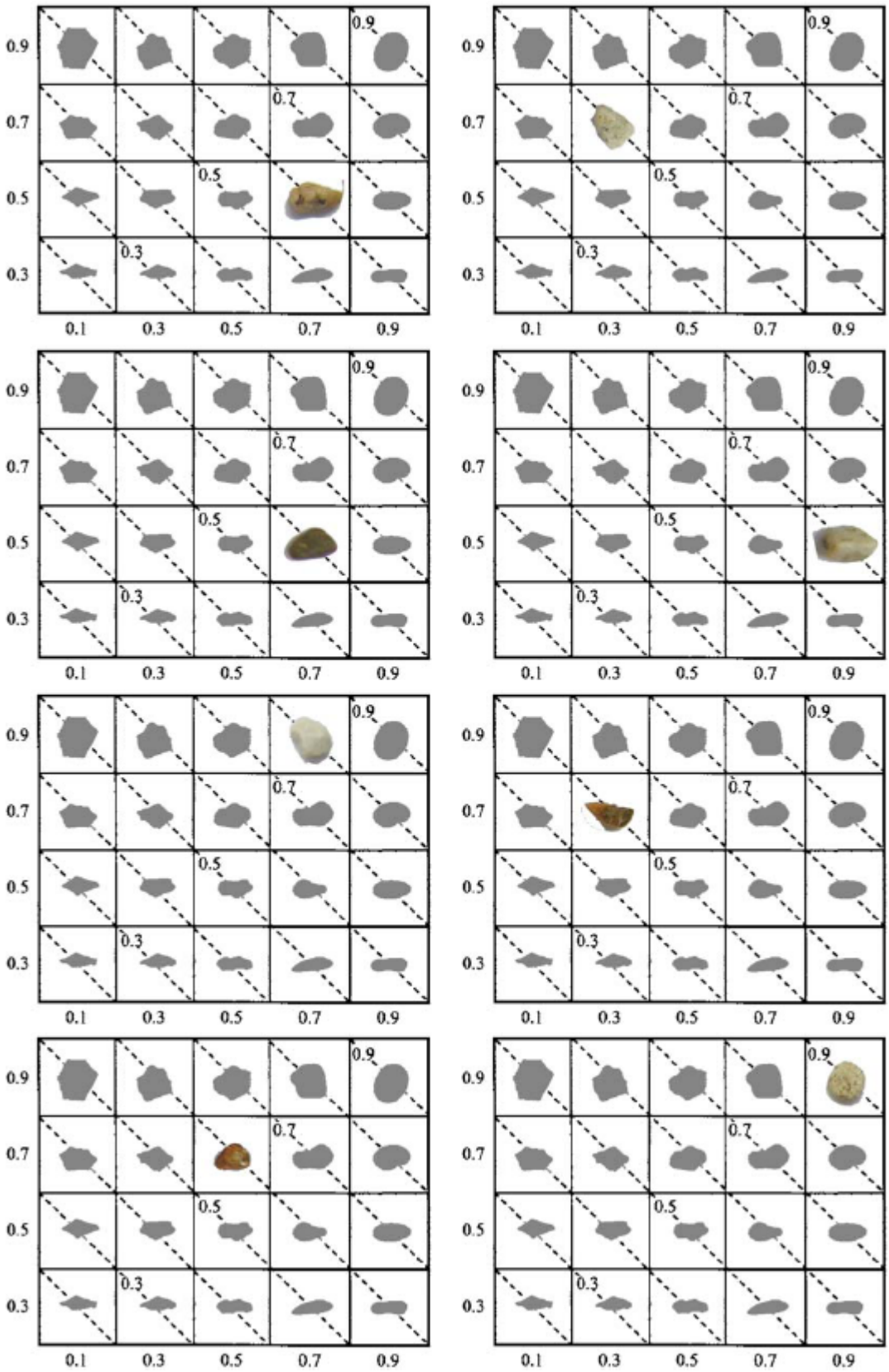


Figure 4.3. Samples of stereomicroscope photographs on shape determination chart (cont.)

4.1. The Law of Large Numbers

According to the probability theorem of law of large numbers, the average of a sample approaches the mean of the population as the sample size increases. The number of grains that are examined is selected as 30 according to law of large numbers, therefore a brief description of the theory is given here, taken from Moore and McCabe (2003).

The probability distribution of a random variable X, like a distribution of observations, has a mean μ_x and a standard deviation σ_x.

If X is a discrete random variable taking values $x_1, x_2, ..., x_k$ with probabilities $p_1, p_2, ..., p_k$ the mean and variance can be computed from its distribution as follows:

$$\mu_x = x_1 p_1 + x_2 p_2 + \cdots + x_k p_k \tag{2.3}$$

$$\sigma_x^2 = \left(x_1 - \mu_x\right)^2 p_1 + \left(x_2 - \mu_x\right)^2 p_2 + \cdots + \left(x_k - \mu_x\right)^2 p_k \tag{2.4}$$

The mean and variance of a continuous random variable can be computed from the density curve, but to do so require more advanced mathematics.

The mean of a random variable is by definition the average outcome of the random variable as computed from the distribution. It is a striking fact that the mean of a random variable is also the average outcome in a different sense. If it is actually observed a large number outcomes of a random variable and calculated their mean (arithmetic average), this random mean will be close to the fixed mean of the distribution.

Suppose that four coins are tossed repeatedly and the number X of heads obtained in each trial is recorded. A computer is used to toss four coins 1000 times and to record the number of heads among the four coins on each trial. Then it is found that the relative frequency of the outcome “exactly two heads” after each trial. The result of the few trials were

Table 4.4. The result of first 6 trials of the toss of four coins

Trial	Outcome	Relative frequency of exactly 2 heads
1	3 heads	$\frac{0}{1}=0$
2	0 heads	$\frac{0}{2}=0$
3	0 heads	$\frac{0}{3}=0$
4	2 heads	$\frac{1}{4}=.25$
5	4 heads	$\frac{1}{5}=.20$
6	2 heads	$\frac{2}{6}=.33$

The first toss gave $X=3$, the second toss $X=0$, then another 0, then 2, 4, 2, and so on. The relative frequency of each outcome in many repetitions will be close to its probability as Figure 4.4 illustrates for the outcome $\{X=2\}$.

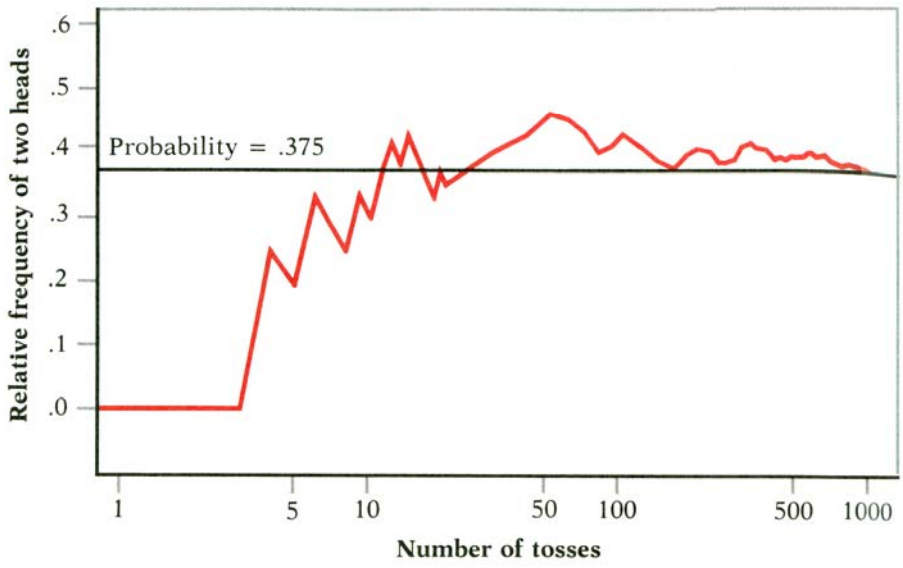


Figure 4.4. The long term behavior of the relative frequency of two heads in many tosses of four coins. The relative frequency approaches the probability 0.375.

The probabilities of all possible outcomes make up the probability distribution of discrete random variable X. What happens to the average number of heads observed? The numbers of heads obtained on each of the first *n* trials form *n* observations. The average number of heads in the first *n* trials is the familiar mean $\bar{x}$ of these observations. The mean $\bar{x}$ is a random variable that takes different values if the tosses are repeated. Here are the values of observations and the mean $\bar{x}$ of all observations to date after each of the first few trials.

Table 4.5. The mean $\bar{x}$ of all observations to date after each of the first few trials

Trial	Outcome	Average number of heads per trial
1	3	$\bar{x} = \frac{3}{1} = 3.00$
2	0	$\bar{x} = \frac{3}{2} = 1.50$
3	0	$\bar{x} = \frac{3}{3} = 1.00$
4	2	$\bar{x} = \frac{5}{4} = 1.25$
5	4	$\bar{x} = \frac{9}{5} = 1.80$
6	2	$\bar{x} = \frac{11}{6} = 1.83$

Figure 4.5 shows the behavior of $\bar{x}$ as the number of trials *n* increases. At first the value of $\bar{x}$ is unstable, but in the long run observed mean $\bar{x}$ approaches and remains close to the distribution mean $\mu_x = 2$. After 100 trials $\bar{x} = 1.86$; at the end of our series of 1000 tosses of four coins $\bar{x} = 2.012$. If the work is repeated, a different sequence of outcomes would be obtained and the graph of the progress of $\bar{x}$ would differ from Figure 4.5. But $\bar{x}$ will always approach $\mu_x = 2$ ever more closely as the number of trial grows.

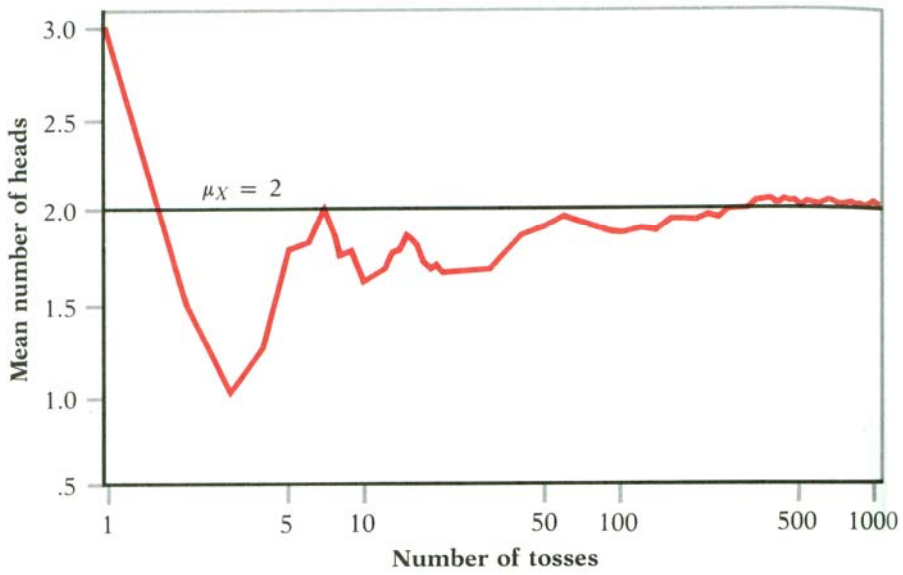


Figure 4.5. The long term behavior of the mean outcome of many trials. The mean number of heads $\bar{x}$ observed when four coins are tossed many times approaches the mean $\mu_x = 2$ of the probability distribution.

Starting from the basic laws o probability, it can actually be proved that the sample mean outcome calculated from repeated independent observations of a random variable must approach the mean of the distribution. It should be noticed, though, that the behavior of $\bar{x}$ is similar to intuitive idea of probability – in long run, relative frequencies of outcomes get close to the probability distribution, and the average outcome gets close to the distribution mean. These facts, especially when they are considered as mathematical results that can be derived from basic laws of probability, are called the law of large numbers. An essential requirement for the law of large numbers to apply is that the successive trials of the random phenomenon be independent. If a coin is tossed by a magician who can influence whether it falls heads or tails, the law of large numbers may not apply. By looking at past outcomes and by manipulating the coin, the magician can change the long term relative frequency of heads.

5. ANGLE OF REPOSE

The angle of repose is a parameter related to shear strength of soils in their loosest state. In this chapter, the definition of angle of repose and its usage in geotechnical engineering applications, experimental techniques used to obtain it, and the results of the angle of repose experiments will be presented.

5.1. Definition of Angle of Repose

Angle of repose is an engineering property of granular materials. It is the maximum angle of a stable slope determined by friction, cohesion and the shape of the particles.

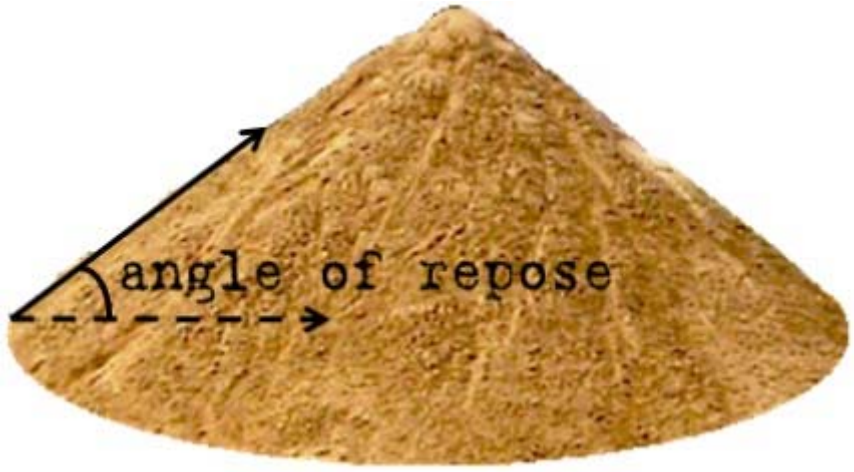


Figure 5.1. Angle of repose

When granular materials are poured onto a horizontal surface, a conical pile will form. The internal angle between the surface of the pile and the horizontal surface is known as the angle of repose and is related to the density, surface area and shapes of the particles, and the coefficient of friction of the material. Material with low angle of repose forms flatter piles than material with high angle of repose. In other words, the angle of repose is the angle a pile forms with the ground.

In soil mechanics, the angle of repose is defined as the maximum slope angle at which a material is stable. Earth masses are generally retained by structures when necessary, but there are many situations in which they are left unretained. The inclination of the slope must be small enough for the earth mass to be stable. The principles of limit equilibrium are valid for both retained and unretained slopes of earth mass. The steepest inclination of a mass in terms of angle with the horizontal when poured by direct pluviation is the measure of the angle of repose.

Parts (a) and (b) of Figure 5.2 shows two typical processes by which a slope is formed in a granular soil. In (a) an embankment is being formed by end dumping from a truck; in (b) sand or some other stockpiled material is dropped from a chute or from the end of a conveyor belt. In both of these situations, the material will tumble down the slope. From time to time during dumping, material which has already come to rest on the slope will start moving again; i.e., a mass of material, with a thickness small compared to the height of the slope, will slide down the slope. The inclination of the slope once dumping has ceased – the maximum slope at which the material is stable – is called the angle of repose. (Lambe and Whitman, 1969).

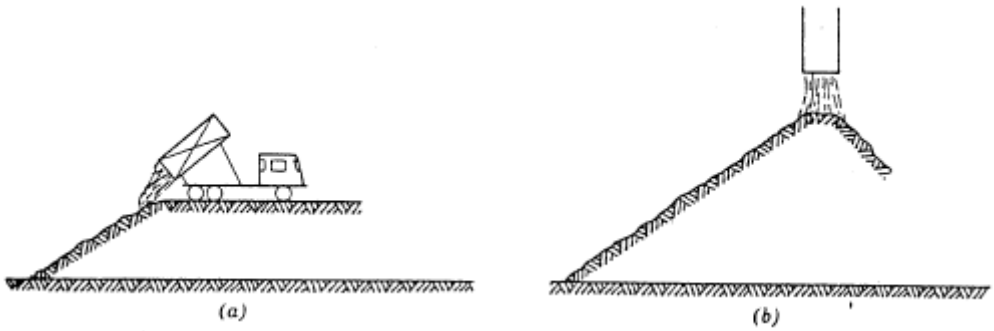


Figure 5.2. Formation of slope (Lambe and Whitman, 1969)

5.2. Experimental Method of Obtaining Angle of Repose

By definition, angle of repose is an easy parameter that can be found by laboratory testing or can be also found in-situ by direct pluviation of sand on a flat surface. Several previous studies have been published and there are several experimental methodologies of obtaining angle of repose. Two of them are referenced here.

The details of the measuring device proposed by Miura et al. (1997), is given in Figure 5.3, and 5.4. The pedestal with a depression and the ring are made of brass, upon which the conical heap is formed. The formation of the sand heap was as follows.

- Set the pedestal and the ring with the spacer so that the upper surface of the ring is level with the top of the pedestal.
- Form the conical heap on the pedestal and the ring with sufficient material in order to cover the pedestal; the material is placed with the funnel, where the height of fall is zero.
- Lower the ring statically by pulling out the spacer very slowly.
- Measure the height H and the base width D_p and calculate the angle of repose ϕ_{rep}.

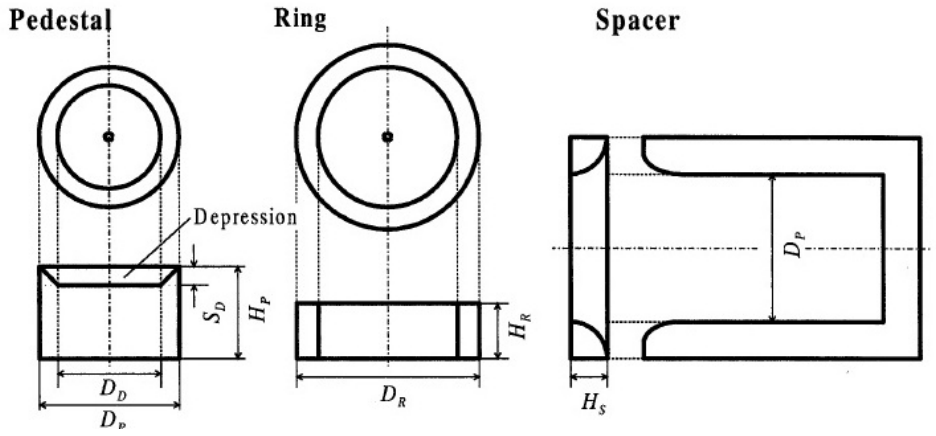


Figure 5.3. Device for measuring the angle of repose ϕ_{rep} : pedestal with depression, ring and spacer (Miura et al. 1997)

Another way of conducting the experiment is proposed by Ghazavi et al. (2008), and the details of the testing apparatus and method can be found in the related reference. In this method, the sand is poured from a determined height, into a tank of 70×70 cm in plan (Figure 5.5). Vertical rods are used to facilitate a variation of height of sand pouring in the tank. A separate storage was used to feed the sand into the tank. After the sand is poured, height and eight radius points of sand cone are obtained and the angle of repose is calculated.

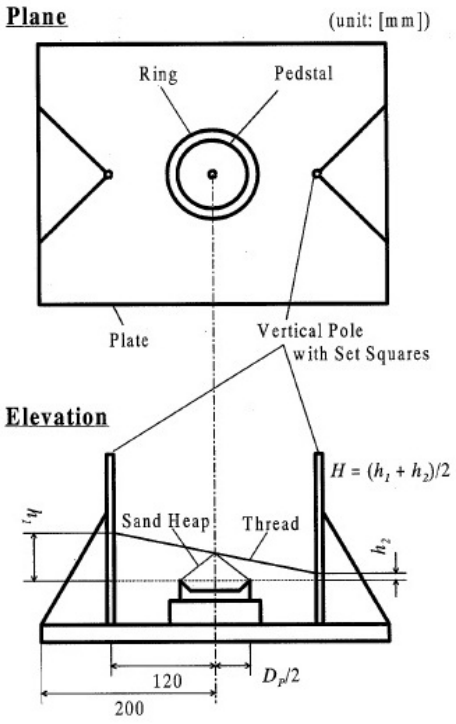


Figure 5.4. Device for measuring the angle of repose ϕ_{rep} : plate with scaled poles (Miura et al. 1997)



Figure 5.5. Apparatus for determining sand repose angle (Ghazavi et al. 2008).

The angle of repose test is not a standardized test therefore; the method used in this study is not same as both of the methods given above. There are similar but different stages in the application of the test. The factors that will influence the angle of repose other than the properties of soil used are the end opening of the funnel that controls the rate of flux,

the drop height of sand grains, the amount of material used, and frictional property of the base plate.

The funnel used in the experiments can be seen in Figure 5.6. The inner diameter of the tip of the funnel (the narrowest cross-section) is 9 mm. The inner diameter of the top part (the widest cross-section) is 100 mm. The height of the funnel is 95 mm, and the height of the narrow tip is 35 mm.



Figure 5.6. The funnel used in experiment

The drop height is fixed by positioning the funnel 200 mm above the base plate. A frame consisting of vertical wooden blocks and steel beams is used to place the funnel standing still into a ring shaped steel collar (Figure 5.7). The base plate is made of plastic, and there is a metric axis system on the base. The position of the tip of funnel is adjusted so that it coincides with the origin of the axis of the base plate, so the first grain dropping hits near the origin point on the base plate. That enables easy calculation of the diameter of the pile formed.

Every experiment is conducted using 750 grams of clean sand soil. The frictional effect of the plastic base plate is ignored in this study.

The properties of the equipments used in the angle of repose test are given above. When the experimental setup is ready, by using a pitcher, 750 g of soil is poured from the funnel. At the beginning the tip of the funnel is closed by finger until the funnel is full (Figure 5.8), to have a constant rate of flow. Material is added continuously until finishing

all of the soil in the pitcher (Figure 5.9). From side and top of the pile formed, photographs are taken (Figure 5.10 and Figure 5.11). The diameter readings are taken from the axis on the base plate (Diameter reading can be made from the top view picture). The height of the pile formed is measured by using calipers.

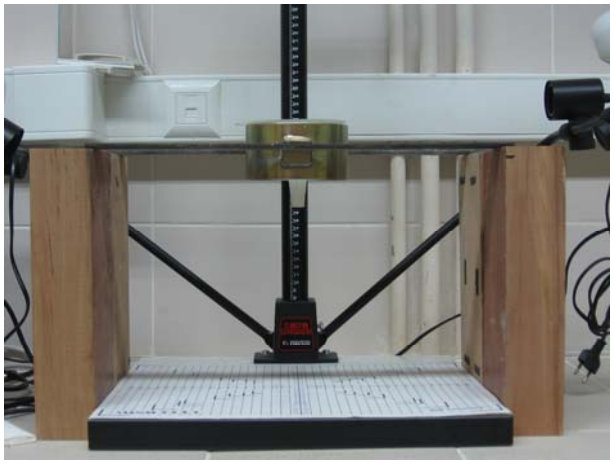


Figure 5.7. The frame used in angle of repose experiment



Figure 5.8. Pouring of the sand

It is observed that insertion of the calipers from the crest of the slope causes deformation. The soil forming the pile is in the loosest state, and at the limit of the shear strength, therefore any additional stress given when inserting calipers will fail the crest part. Precise reading can not be taken by caliper. A measuring device using laser light is advised if it is necessary to measure the height. The angle of repose in this study is found by directly drawing lines on the side view pictures of the pile formed.

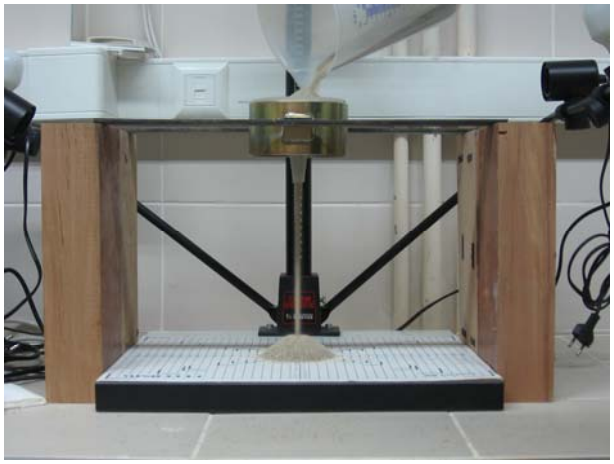


Figure 5.9. Flow of sand



Figure 5.10. Side view of the pile formed

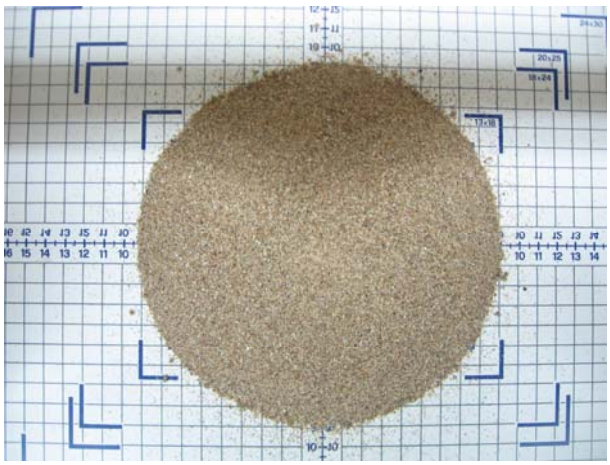


Figure 5.11. Top view of the pile formed

5.3. Results of Angle of Repose Experiments

Two sets of experiments are conducted using five different sand specimens selected. The five specimens are namely Sile Sand, Silivri Sand, Crushed Sand, Meric River Sand, and Sakarya Sand. The properties of the soils are explained in Section 3. The first set is conducted using 750 grams of uniformly graded sand specimen that falls between No.16 and No.40 sieve sizes. The second set is conducted by mixing 250 grams of soil for each grading, No.10 – No.16, No.16 – No.40, and No.40 – No.70, respectively. Therefore, first set is conducted on uniformly graded specimens, whereas second set is conducted on well-graded specimens. The effect of grading is also investigated in the study.

There is an exception for the Sile Sand about the grading. After the results of sieve analysis of Sile Sand, no samples are obtained above No.16 sieve. Therefore two lower grades (No.16 – No.40 and No.40 – No.70) are mixed in equal amount that is 375 grams. It is also modeled in the same manner in PFC2D program.

The measurement was made by drawing a line and measuring the angle with the horizontal near the mid-height of the slope formed (Figure 5.12). Two measurements were taken from the right and left sides, and the average of the two angles is selected as the value of angle of repose.



Figure 5.12. Measurement technique of the angle of repose

The results of the five sand specimens with uniform and well grading are tabulated in Table 5.1.

Table 5.1. Angle of repose values obtained from experiments

	Angle of Repose (°)	
	Uniformly Graded	**Well Graded**
	Between sieves No. 16 and No. 40	**Between Sieves No.10 and No. 70**
Sile Sand	31	32
Silivri Sand	31.5	35
Crushed Sand	36.5	36.5
Meric Sand	36	35
Sakarya Sand	34.5	34.5

6. DISTINCT ELEMENT MODELING USING PFC2D[1]

Mankind has always used models, which are in effect a simplified picture of reality, as a tool to solve problems. The model will never contain all the features of the real system, because, and then, it would be the real system itself. However, it is important that the model contains the characteristic features that are essential in the context of the problem to be solved or described. Models have some certain features: they are useful instruments in the survey of complex systems, they can be used to reveal system properties, they reveal weaknesses in our knowledge and can therefore be used to set up research priorities, they are useful in tests of scientific hypothesis (Jorgensen et al., 2003).

Granular materials, like sand or gravel, are composed of distinct particles interacting at contact points. Within such materials, the contact network provides internal transmission of forces, whose averaging over a sufficiently wide volume allows us to define a continuum-equivalent stress tensor. On the other hand, local kinematics is described by translational and spin velocity of particles: the non-uniform distribution of these variables gives rise to macroscopic deformations. Local behavior is ruled by simple principles: contact shear force cannot overcome a threshold fixed by Coulomb's law, and contacts are only active in compression. These two limitations represent the main source of weakness of granular materials; moreover, they can be considered as responsible for the complex macro-behavior of sands, since they allow important structure changes during loading. Nevertheless, on a global scale, granular materials are usually considered as continua, neglecting their discrete nature; as a consequence, constitutive models are based on macro-mechanical observations, and granular materials can therefore be treated in the framework of elastoplasticity. Probably owing to the scale of approach, such models either are unable to reproduce real sand behavior under complex load histories or need the introduction of several internal parameters, like plastic deformation and hardening variables, whose physical meaning is generally not clearly defined (Calvetti and Lanier, 1997).

[1] Notations and derivations are adapted from PFC2D Version 4.0 User's Manuals.

The user manuals of the program PFC2D is used as main reference for describing the theoretical background for the distinct element method and the mathematics of the model. Other references are cited in related parts.

6.1. The Distinct Element Method

The distinct element method is a numerical model capable of describing the mechanical behavior of assemblies of discs and spheres. The method is based on the use of an explicit numerical scheme in which the interaction of the particles is monitored contact by contact and the motion of the particles modeled particle by particle (Cundall and Strack, 1979).

The stress-strain behavior of a dense granular assembly consists of two parts: the rearrangement of the particles on the one hand, and their individual elastic or plastic deformation on the other (Kadau et.al., 2006).

PFC2D models the movement and interaction of stressed assemblies of rigid circular particles using the distinct-element method (DEM). The DEM was introduced by Cundall (1971) for the analysis of rock-mechanics problems and then applied to soils by Cundall and Strack (1979). A thorough description of the method is given in the two-part paper of Cundall (1988) and Hart et al. (1988). PFC2D is classified as a discrete element code based on the definition in the review of Cundall and Hart (1992) since it allows finite displacements and rotations of discrete bodies, including complete detachment, and recognizes new contacts automatically as the calculation progresses. PFC2D can be viewed as a simplified implementation of the DEM because of the restriction to rigid circular particles.

In the DEM, the interaction of the particles is treated as a dynamic process with states of equilibrium developing whenever the internal forces balance. The contact forces and displacements of a stressed assembly of particles are found by tracing the movements of the individual particles. Movements result from the propagation through the particle system of disturbances caused by specified wall and particle motion and/or body forces.

This is a dynamic process in which the speed of propagation depends on the physical properties of the discrete system.

The dynamic behavior is represented numerically by an explicit timestepping algorithm, using a central-difference scheme to integrate accelerations and velocities. The DEM is based upon the idea that the timestep chosen may be so small that, during a single timestep, disturbances cannot propagate from any particle further than its immediate neighbors. Then, at all times, the forces acting on any particle are determined exclusively by its interaction with the particles with which it is in contact. Since the speed at which a disturbance can propagate is a function of the physical properties of the discrete system, the timestep can be chosen to satisfy the above constraint. The use of an explicit, as opposed to an implicit, numerical scheme makes it possible to simulate the nonlinear interaction of a large number of particles without excessive memory requirements or the need for an iterative procedure.

The calculations performed in the DEM alternate between the application of Newton's second law to the particles and a force-displacement law at the contacts. Newton's second law is used to determine the motion of each particle arising from the contact and body forces acting upon it, while the force-displacement law is used to update the contact forces arising from the relative motion at each contact. The presence of walls in PFC2D requires only that the force-displacement law account for ball-wall contacts. Newton's second law is not applied to walls, since the wall motion is specified by the user.

6.2. The PFC2D Particle Flow Model

A general particle-flow model simulates the mechanical behavior of a system comprised of a collection of arbitrarily shaped particles. (Note that the term "particle," as used here, differs from its more common definition in the field of mechanics, where it is taken as a body whose dimensions are negligible and therefore occupies only a single point in space. In the present context, the term "particle" denotes a body that occupies a finite amount of space.) The model is composed of distinct particles that displace independently from one another, and interact only at contacts or interfaces between the particles. If the

particles are assumed to be rigid, and the behavior of the contacts is characterized using a soft contact approach in which a finite normal stiffness is taken to represent the measurable stiffness that exists at a contact, then the mechanical behavior of such a system is described in terms of the movement of each particle and the inter-particle forces acting at each contact point. Newton's laws of motion provide the fundamental relationship between particle motion and the forces causing that motion. The force system may be in static equilibrium—in which case, there is no motion— or it may be such as to cause the particles to flow.

More complex behavior can be modeled by allowing the particles to be bonded together at their contact points such that, when the inter-particle forces acting at any bond exceed the bond strength, that bond is broken. This allows tensile forces to develop between particles. One can then model the interaction of these bonded "blocks," including the formation of cracks that may cause blocks to fragment into smaller blocks.

PFC2D provides a particle-flow model containing the following assumptions.

1. The particles are treated as rigid bodies but deform locally at contact points in which a finite normal and shear stiffnesses are taken to represent measurable contact stiffnesses.
2. The contacts occur over a vanishingly small area (i.e., at a point).
3. Behavior at the contacts uses a soft-contact approach, wherein the rigid particles are allowed to overlap one another at contact points.
4. The magnitude of the overlap is related to the contact force via the force-displacement law, and all overlaps are small in relation to particle sizes.
5. Bonds can exist at contacts between particles.
6. All particles are circular. However, the clump logic supports the creation of super-particles of arbitrary shape. Each clump consists of a set of overlapping particles that act as a rigid body with a deformable boundary.

A PFC2D model consists of a two-dimensional collection of circular particles. The PFC2D "world" is two dimensional in nature (i.e., only two force components and one moment component exist in a PFC2D model, as opposed to the three force components and

three moment components that exist in a three-dimensional particle assembly). The out-of-plane force component and the two in-plane moment components are not considered in any way in the equations of motion or in the force-displacement laws. Therefore, the question of exactly what, in a three-dimensional sense, is being simulated in a PFC2D model is a matter of interpretation. For example, one might consider the PFC2D model to be simulating a collection of variable-radius cylinders. Alternatively, one might consider the PFC2D model to be simulating a collection of variable-radius spheres whose centroids all lie upon the same plane.

The assumption of particle rigidity is a good one when most of the deformation in a physical system is accounted for by movements along interfaces. The deformation of a packed-particle assembly, or a granular assembly such as sand, as a whole, is described well by this assumption, since the deformation results primarily from the sliding and rotation of the particles as rigid bodies, and the opening and interlocking at interfaces, and not from individual particle deformation. Precise modeling of particle deformation is not necessary to obtain a good approximation of the mechanical behavior for such systems.

In addition to traditional particle-flow applications, PFC2D can also be applied to the analysis of solids subjected to prescribed boundary and initial conditions. In such models, the continuum behavior is approximated by treating the solid as a compacted assembly of many small particles. Measures of stress and strain rate can be defined as average quantities over a representative measurement volume for such systems. This allows one to estimate interior stresses for granular materials, such as soils, or solid materials, such as rock or plastics formed by powder compaction.

In addition to circular particles, referred to hereafter as “balls,” the PFC2D particle-flow model also includes “walls.” Walls allow one to apply velocity boundary conditions to assemblies of balls for purposes of compaction and confinement. The balls and walls interact with one another via the forces that arise at contacts. The equations of motion are satisfied for each ball. However, the equations of motion are not satisfied for each wall i.e., forces acting on a wall do not influence its motion. Instead, its motion is specified by the user and remains constant regardless of the contact forces acting upon it. Also, contacts may not form between two walls. Thus, contacts are either ball-ball or ball-wall.

6.3. Force Displacement Law

The force-displacement law derives the contact force acting on two entities in contact to the relative displacement between the entities. For both ball-ball and ball-wall contacts, this contact force arises from contact occurring at a point (modeled using the soft-contact approach). For ball-ball contact, an additional force and moment arising from the deformation of the cementatious material represented by a parallel bond can also act on each particle. Only the calculation of the contact force arising from the contact at a point is described in this section.

The force-displacement law operates at a contact and can be described in terms of a contact point $x_i^{[C]}$, lying on a contact plane that is defined by a unit normal vector, n_i. (n_i lies in the plane of the PFC2D model.) The contact point is within the interpenetration volume of the two entities. For ball-ball contact, the normal vector is directed along the line between ball centers. For ball-wall contact, the normal vector is directed along the line defining the shortest distance between the ball center and the wall. The contact force is decomposed into a normal component acting in the direction of the normal vector and a shear component acting in the contact plane. (The shear component also lies in the plane of the PFC2D model.) The force-displacement law relates these two components of force to the corresponding components of the relative displacement via the normal and shear stiffnesses at the contact.

The force-displacement law is described for both ball-ball and ball-wall contacts. For ball-ball contact, the relevant equations are presented for the case of two spherical particles, labeled A and B in Figure 6.1. For ball-wall contact, the relevant equations are presented for the case of a spherical particle and a wall, labeled b and w, respectively, in Figure 6.2. In both cases, U^n denotes overlap.

For ball-ball contact, the unit normal, n_i, that defines the contact plane is given by

$$n_i = \frac{x_i^{[B]} - x_i^{[A]}}{d} \quad \text{(ball-ball)} \tag{6.1}$$

where $x_i^{[A]}$ and $x_i^{[B]}$ are the position vectors of centers of balls A and B, and d is the distance between the ball centers:

$$d = \left| x_i^{[B]} - x_i^{[A]} \right| = \sqrt{\left(x_i^{[B]} - x_i^{[A]} \right)\left(x_i^{[B]} - x_i^{[A]} \right)} \quad \text{(ball-ball)} \tag{6.2}$$

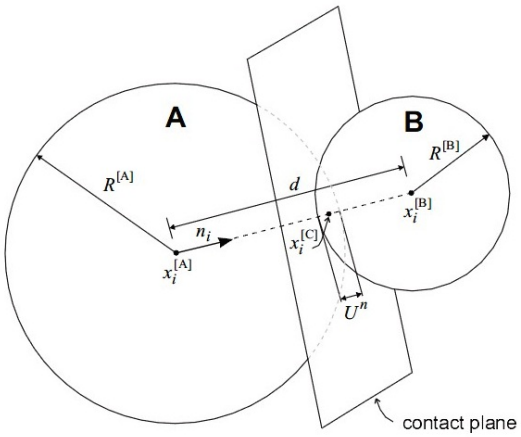


Figure 6.1. Notation used to describe ball-ball contact

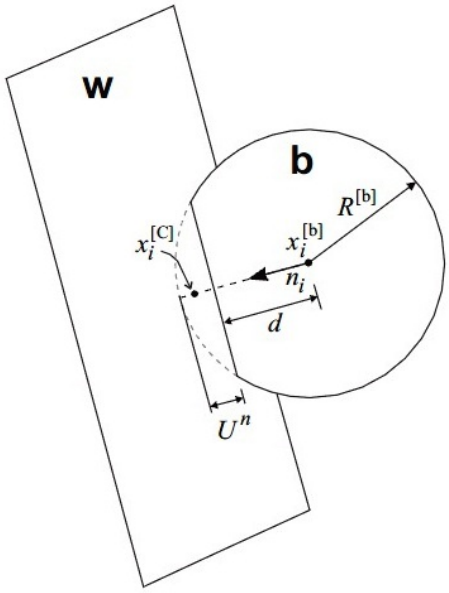


Figure 6.2. Notation used to describe ball-wall contact

Note that n_i corresponds with position vectors at time $t-\Delta t/2$, to preserve the time-centering of equations.

For ball-wall contact, n_i is directed along the line defining the shortest distance, d, between the ball center and the wall. This direction is found by mapping the ball center into a relevant portion of space defined by the wall. The idea is illustrated in Figure 6.3 for a two-dimensional wall composed of two line segments AB and BC. All space on the active side of this wall can be decomposed into five regions by extending a line normal to each wall segment at its endpoints. If the ball center lies in regions 2 or 4, it will contact the wall along its length, and n_i will be normal to the corresponding wall segment. However, if the ball center lies in regions 1, 3, or 5, it will contact the wall at one of its endpoints, and n_i will lie along the line joining the endpoint and the ball center.

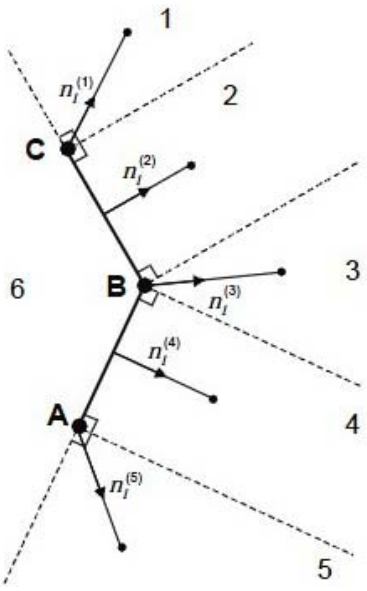


Figure 6.3. Determination of normal direction for ball-wall contact

The overlap, U^n, defined to be the relative contact displacement in the normal direction, is given by

$$U^n = \begin{cases} R^{[A]} + R^{[B]} - d, & \text{(ball-ball)} \\ R^{[b]} - d, & \text{(ball-wall)} \end{cases} \tag{6.3}$$

where $R^{[\Phi]}$ is the radius of ball Φ.
The location of contact point is given by

$$x_i^{[C]} = \begin{cases} x_i^{[A]} + \left(R^{[A]} - \frac{1}{2} U^n \right) n_i, & \text{(ball-ball)} \\ x_i^{[b]} + \left(R^{[b]} - \frac{1}{2} U^n \right) n_i, & \text{(ball-wall)} \end{cases} \tag{6.4}$$

The contact force vector, F_i, (which represents the action of ball A on ball B for ball-ball contact, and the action of the ball on the wall for ball-wall contact), can be resolved into normal and shear components with respect to the contact plane as

$$F_i = F_i^n + F_i^s \tag{6.5}$$

where F_i^n and F_i^s denote the normal and shear component vectors, respectively.

The magnitude of the normal contact force is calculated by

$$F^n = K^n U^n \tag{6.6}$$

where K^n is the normal stiffness [force/displacement] at the contact. The value of K^n is determined by the current contact-stiffness model.

Note that the normal stiffness, K^n, is a secant modulus in that it relates total displacement and force. The shear stiffness, k^s, on the other hand, is a tangent modulus in that it relates incremental displacement and force. An uppercase K will be used to denote a secant modulus, and a lowercase k will be used to denote a tangent modulus. The computation of normal contact force from the geometry alone makes the codes less prone to numerical drift, and able to handle arbitrary placement of balls and changes in ball radii after a simulation has begun. Note that Equation (6.3) is evaluated in double precision.

The shear contact force is computed in an incremental fashion. When the contact is formed, the total shear contact force is initialized to zero. Each subsequent relative shear-displacement increment results in an increment of elastic shear force that is added to the current value. The motion of the contact is considered during this procedure by updating n_i and $x_i^{[C]}$ every timestep.

The relative shear motion at the contact, or the shear contact velocity, V_s (which is defines as the shear velocity of ball B relative to ball A at the contact point for ball-ball contact, and is defined as the shear velocity of the wall relative to the ball at the contact point for ball-wall contact), is given by

$$V^s = \left(\dot{x}_i^{\left[\Phi^2\right]} - \dot{x}_i^{\left[\Phi^1\right]} \right) t_i - \omega_3^{\left[\Phi^2\right]} \left| x_k^{[C]} - x_k^{\left[\Phi^2\right]} \right| - \omega_3^{\left[\Phi^1\right]} \left| x_k^{[C]} - x_k^{\left[\Phi^1\right]} \right| \tag{6.7}$$

where $\dot{x}_i^{\left[\Phi^j\right]}$ and $\omega_3^{\left[\Phi^j\right]}$ are the translational and rotational velocity, respectively, of entity Φ^j given by

$$\left\{\Phi^1, \Phi^2\right\} = \begin{cases} \{A, B\}, & (\text{ball-ball}) \\ \{b, w\}, & (\text{ball-wall}) \end{cases} \tag{6.8}$$

and $t_i = \{-n_2, n_1\}$. (Note that $\omega_3^{[w]}$ is the rotational velocity of the wall with respect to $x_i^{[w]}$, the center of rotation of the wall).

The shear component of the contact displacement increment occurring over a timestep of Δt is calculated by

$$\Delta U^s = V^s \Delta t \tag{6.9}$$

and is used to calculate the shear elastic force increment

$$\Delta F^s = -k^s \Delta U^s \tag{6.10}$$

where k^s is the shear stiffness [force/displacement] at the contact. The value of k^s is determined by the current contact stiffness model. The shear stiffness is a tangent modulus, and is thus denoted using a lowercase k.

The new shear contact force is found by summing the old shear force at the start of timestep with the shear elastic force increment

$$F^s \leftarrow F^s + \Delta F^s \leq \mu F^n \tag{6.11}$$

where μ is the friction coefficient.

The values of normal and shear contact force determined by Equations (6.6) and (6.11) are adjusted to satisfy the contact constitutive relations. After this adjustment, the contribution of the final contact force and moment on the two entities in contact is given by

$$\begin{aligned}
&F_i = F^n n_i + F^s t_i \\
&F_i^{\left[\Phi^1\right]} \leftarrow F_i^{\left[\Phi^1\right]} - F_i \\
&F_i^{\left[\Phi^2\right]} \leftarrow F_i^{\left[\Phi^2\right]} + F_i \\
&M_3^{\left[\Phi^1\right]} \leftarrow M_3^{\left[\Phi^1\right]} - e_{3jk}\left(x_j^{[C]} - x_j^{\left[\Phi^1\right]}\right)F_k \\
&M_3^{\left[\Phi^2\right]} \leftarrow M_3^{\left[\Phi^2\right]} - e_{3jk}\left(x_j^{[C]} - x_j^{\left[\Phi^2\right]}\right)F_k
\end{aligned} \tag{6.12}$$

where $F_i^{\left[\Phi^j\right]}$ and $M_3^{\left[\Phi^j\right]}$ are the force and moment sums for entity Φ^j from Equation (6.8), and F_i is given by Equation (6.5).

6.4. Law of Motion

The motion of a single rigid particle is determined by the resultant force and moment vectors acting upon it, and can be described in terms of the translational motion of a point in the particle and the rotational motion of the particle. The rotational motion of the

center of mass is described in terms of its position, x_i, velocity, $\dot{x}_i$, and acceleration, $\ddot{x}_i$; the rotational motion of the particle is described in terms of its angular velocity, ω_i, and angular acceleration, $\dot{\omega}_i$.

The equations of motion can be expressed as two vector equations: one relates the resultant force to the translational motion; the other relates the resultant moment to the rotational motion. The equation for translational motion can be written in the vector form:

$$F_i = m\left(\ddot{x}_i - g_i\right) \quad \left(\text{translational motion}\right) \tag{6.13}$$

where F_i is the resultant force, the sum of all externally applied forces acting on the particle; m is the total mass of the particle; and g_i is the body force acceleration vector (e.g., gravity loading).

The equation for rotational motion can be written in the vector form:

$$M_i = \dot{H}_i \tag{6.14}$$

where M_i is the resultant moment acting on the particle, and $\dot{H}_i$ is the angular momentum of the particle. This relation is referred to a local coordinate system that is attached to the particle at its center of mass. If this local system is oriented such that it lies along the principal axes of inertia of the particle, then Equation 6.14 reduces to Euler's equation of motion:

$$\begin{aligned} M_1 &= I_1\dot{\omega}_1 + \left(I_3 - I_2\right)\omega_3\omega_2 \\ M_2 &= I_2\dot{\omega}_2 + \left(I_1 - I_3\right)\omega_1\omega_3 \\ M_3 &= I_3\dot{\omega}_3 + \left(I_2 - I_1\right)\omega_2\omega_1 \end{aligned} \tag{6.15}$$

where I_1, I_2, and I_3 are the principal moments of inertia of the particle; $\dot{\omega}_1$, $\dot{\omega}_2$, and $\dot{\omega}_3$ are the angular accelerations about the principal axes; and M_1, M_2, and M_3 are the components of the resultant moment referred to the principal axes.

For either a spherical or a disk-shaped particle of radius R, whose mass is distributed uniformly throughout its volume, the center of mass coincides with the sphere or disk center. For a spherical particle, any local-axis system attached to the center of mass is a principal-axis system, and the three principal moments of inertia are equal to one another. For a disk-shaped particle whose axis remains in the out-of-plane direction, $\omega_1 = \omega_2 \equiv 0$. Thus, for either of these particles, Equation (6.15) can be simplified and referred to the global-axis system as

$$M_3 = I\dot{\omega}_3 = \left(\beta m R^2\right)\dot{\omega}_3 \quad \left(\text{rotational motion}\right) \tag{6.16}$$

where

$$\beta = \begin{cases} 2/5, & \left(\text{spherical particle}\right) \\ 1/2, & \left(\text{disk-shaped particle}\right) \end{cases} \tag{6.17}$$

The equations of motion, given by Equations (6.13) and (6.16), are integrated using a centered finite-difference procedure involving a timestep of Δt. The quantities $\dot{x}_i$ and ω_3 are computed at the mid-intervals of $t \pm n\Delta t/2$, while the quantities x_i, $\ddot{x}_i$, $\dot{\omega}_3$, F_i, and M_3 are computed at the primary intervals of $t \pm n\Delta t$.

The following expressions can describe the translational and rotational accelerations at time t in terms of the velocity values at mid-intervals. The accelerations are calculated as:

$$\begin{aligned} \ddot{x}_i^{(t)} &= \frac{1}{\Delta t}\left(\dot{x}_i^{(t+\Delta t/2)} - \dot{x}_i^{(t-\Delta t/2)}\right) \\ \dot{\omega}_3^{(t)} &= \frac{1}{\Delta t}\left(\omega_3^{(t+\Delta t/2)} - \omega_3^{(t-\Delta t/2)}\right) \end{aligned} \tag{6.18}$$

Inserting these expressions into Equations (6.13) and (6.16), and solving for the velocities at time $\left(t + \Delta t/2\right)$, results in:

$$\dot{x}_i^{(t+\Delta t/2)} = \dot{x}_i^{(t-\Delta t/2)} + \left(\frac{F_i^{(t)}}{m} + g_i \right) \Delta t$$
$$\omega_3^{(t+\Delta t/2)} = \omega_3^{(t-\Delta t/2)} + \left(\frac{M_3^{(t)}}{I} \right) \Delta t \tag{6.19}$$

Finally, the velocities in Equation (6.19) are used to update the position of the particle center as

$$x_i^{(t+\Delta t)} = x_i^{(t)} + \dot{x}_i^{(t+\Delta t/2)} \Delta t \tag{6.20}$$

The calculation cycle for the law of motion can be summarized as follows. Given the values of $\dot{x}_i^{(t-\Delta t/2)}$, $\omega_3^{(t-\Delta t/2)}$, $x_i^{(t)}$, $F_i^{(t)}$, and $M_3^{(t)}$, Equation (6.19) is used to obtain $\dot{x}_i^{(t+\Delta t/2)}$ and $\omega_3^{(t+\Delta t/2)}$. Then, Equation (6.20) is used to obtain $x_i^{(t+\Delta t/2)}$. The values of $F_i^{t+\Delta t}$ and $M_3^{t+\Delta t}$, to be used in the next cycle, are obtained by application of the force-displacement law.

6.5. Limitations of Two-Dimensional Modeling

There are certain limitations inherent to a two-dimensional discrete element code like PFC2D to model physical phenomena which are three dimensional in nature. The most problematic of these limitations is, in a PFC2D model, only two force components and one moment component exist, as opposed to the three force components and three moment components that exist in a three-dimensional particle assembly. The out-of-plane force component and the two in-plane moment components are not considered in any way in the equations of motion or the force-displacement laws.

6.5.1. Stress and Strain

Stress and strain, as continuous variables, do not exist at each point in a particle assembly, because the medium is discontinuous. In the discrete PFC2D model, contact

forces and particle displacements are computed. These quantities are useful when studying the material behavior on a microscale, but they can not be transferred directly to a continuum model. Therefore, an averaging procedure is employed to compute average stress and strain-rate tensors within a user-defined measurement circle. Averaging procedures are necessary to make the step from the microscale to a continuum. The averaging procedure for stress relates the two in-plane force components acting on each particle in the measurement circle to a force per unit length of particle boundary, which must then be divided by a thickness value in order to obtain a stress quantity.

Most two-dimensional continuum-based codes determine three-dimensional elastic response by enforcing a condition of either plane stress or plane strain through the constitutive relations between stress and strain. A PFC2D model, however, enforces neither of these conditions. The out-of-plane force component and stresses and strains are simply not considered in the equations of motion or in the force-displacement laws. Thus, the out of plane constraint necessary to enforce a state of plane strain is not present.

6.5.2. Packing and Porosity

The porosity computed by PFC2D is and area-based calculation (ratio of total void area to total area), as opposed to the volume-based calculation (ratio of total void volume to total volume) used to define three-dimensional porosity. There is no clear relation between a two-dimensional porosity value and a three-dimensional porosity value for arbitrary assemblies of spherical particles. However, since porosity is a measure of particle packing, the following information about the particle packing in 2D and 3D highlights and explains some of the differences.

It is shown in Deresiewicz (1958) that the closest of all regular packings of uniform spheres in 3D has a porosity of 0.2595, while the closest of all regular packings of uniform circles in 2D has a porosity of 0.0931. In the absence of compressive forces acting on the assembly, these are the theoretical lowest values of porosity obtainable without particle interpenetration. In general, there is more void space remaining in a 3D assembly than in a 2D assembly. In a real material the porosities will be higher, because the particles will have “locked-up” before reaching this optimal packing. If particle arching is known to

occur in a real material, there are many opportunities for arches to form in a 3D assembly than in a 2D assembly. Another difference between 2D and 3D assemblies relates to percolation. Small particles can easily percolate through a 3D assembly comprised of larger particles, but they can never percolate through a packed PFC2D model, regardless of relative particle sizes.

6.5.3. Mass Properties

The mass of each particle is determined by considering the particle to be either a sphere or a disk. By default, balls are treated as spheres. The mass is assigned based on the density, radius and disk thickness. The particle masses affect both the motion calculation (since the inertial properties differ for a disk and a sphere) and the gravity force applied to each particle.

7. TWO DIMENSIONAL MODELLING OF ANGLE OF REPOSE EXPERIMENT

Macroscale strength characteristics of dry granular materials are expressed in terms of material friction angle, whereas in microscale friction coefficient among individual particles, particle shape, particle size determines the shear strength of random assemblies of granular materials. The friction angle of the bulk material is not equal to the contact friction angle between particles. A relation between the friction coefficient of a particle and the peak friction angle of the material assemblage can be demonstrated by running numerical tests to determine the angle of repose of a slope.

Skinner (1969) shows by laboratory testing that the peak friction angle does not increase linearly as a function of particle friction coefficient. When shearing a random assembly of spherical particles it is shown in Skinner's work that both the effective angle of shearing resistance at constant volume and at peak for a given initial porosity do not increase monotonically with increase in the interparticle angle of friction. Both dry and flooded tests are done using glass battolini, steel ball bearings and lead shot samples in a specially developed shearing device. Skinner comes to two main conclusions that are firstly during shear particle rolling can occur, and second that shear strength need not necessarily change if the interparticle friction changes.

The friction coefficient between interacting grains obviously will affect the shear strength of soils, although it is not the only cause of shearing resistance. Particle size and shape are the two other important factors that affect shearing resistance. The effects of these factors on shear strength of the assembly can be modeled in the distinct element program. In distinct element modeling of angle of repose test an assembly of balls is created within a defined space. The radiuses of the balls are specified according to the gradation of the soil sample. The specific gravity of soil solids are used to give density values to the balls. Then these balls are replaced with clumps to include the effect of particle shape into the model. Afterwards, the only remaining parameter missing in the definition of the model is the friction coefficient between contacting grains. This is an unknown parameter that will be found by comparing the experimental findings of angle of

repose test and the results of the numerical model. Therefore the relationship between angle of repose value of sands and the interparticle friction coefficient can be searched in this part of study.

A stepwise procedure is followed during modeling starting from simple idealized models consisting of only balls with different interparticle friction coefficient. It progresses with trials of clumps consisting of two balls representing the shape of the grains. Then the shape parameters found by taking photographs of individual grains are employed into the distinct element code and clumps are generated which reflects the sphericity and angularity of the real grains. At this last stage four balls are used to generate one clump. This is done for all five different sands.

7.1. Simple Idealized Model Consisting of Balls with Different Friction Coefficient

When idealizing a physical system for numerical analysis, it is more efficient to construct and run simple test models first, before building the detailed model. Simple models should be created at the earliest possible stage in a project to generate both data and understanding. The results can provide further insight into the conceptual picture of the system.

For the reasons stated above two assemblies consisting of balls with same physical properties except the interparticle friction coefficient are tested. In the first run, the balls have interparticle friction coefficient, $\mu = 0.6$, and in the second run $\mu = 0.9$. Therefore pure effect of friction coefficient independent of grain shape was observed. It is founded that angle of repose values are 18° and 25° for $\mu = 0.6$ and $\mu = 0.9$, respectively as shown in Figures 7.1 and 7.2. Therefore angle of repose increases with increasing value of friction coefficient.



Figure 7.1. Observed pile for $\mu = 0.6$



Figure 7.2. Observed pile for $\mu = 0.9$

Another comparison is made about problem scale properties. Radii of the spheres are multiplied by 10 and 100, and it is observed that the piles forming have same geometries. Therefore it can be concluded that scaling the radiuses does not change the packing of the spheres unless there is no change in the radius distribution of the particles.

7.2. Utilization of Clumps to Reflect Particle Shape

Several particles may be bonded together to form a cluster that can act like a particle of non-uniform shape. A clump behaves as a rigid body (i.e., the particles comprising the clump remain at a fixed distance from each other). Contacts internal to the clump are skipped during the calculation cycle, resulting in a saving of computer time compared to a similar calculation in which all contacts are active. However, contacts with particles external to the clump are not affected (i.e., such contacts will develop when the particles comprising the boundary of a clump come into contact with other particles). Particles within a clump may overlap to any extent; contact forces are not generated between these particles, but any contact forces that exist when the clump is created or when a particle is added to the clump will be preserved unchanged during cycling. Thus, a clump acts as a rigid body (with a deformable boundary) that will not break apart, regardless of the forces acting upon it. In this sense, a clump differs from a group of particles that are bonded to one another.

In Section 4, the grain shapes of the particles are defined in terms of sphericity and roundness values. Clumps are generated for the sample soils taking into account the values of roundness and sphericity. The sphericity value is related to particles height, width, and length, therefore it is possible and easy to obtain when creating clumps. Obtaining roundness is not that easy, because it is related to the surface features and angular grains

can not be created using circles. Closer values of roundness can be obtained if the number of balls used in the clump is increased. The runtime increases dramatically if too many balls are used in a single clump. Therefore clumps consisting of four balls are used to model the grain shapes of the five different sand specimens. The chart used to obtain the values of roundness and sphericity (Figure 4.1) is used here for clump generation.

The shape representations of the grains with values of roundness and sphericity are used as a template for the clump. Radius and relative position of four circles is tried to be as close as the shape on the chart (Figure 7.3). Mathematical description of roundness does not hold in this technique but qualitatively grain shapes are represented. The combined effects of roundness and roughness is reflected in the coefficient of friction used in the distinct element models.

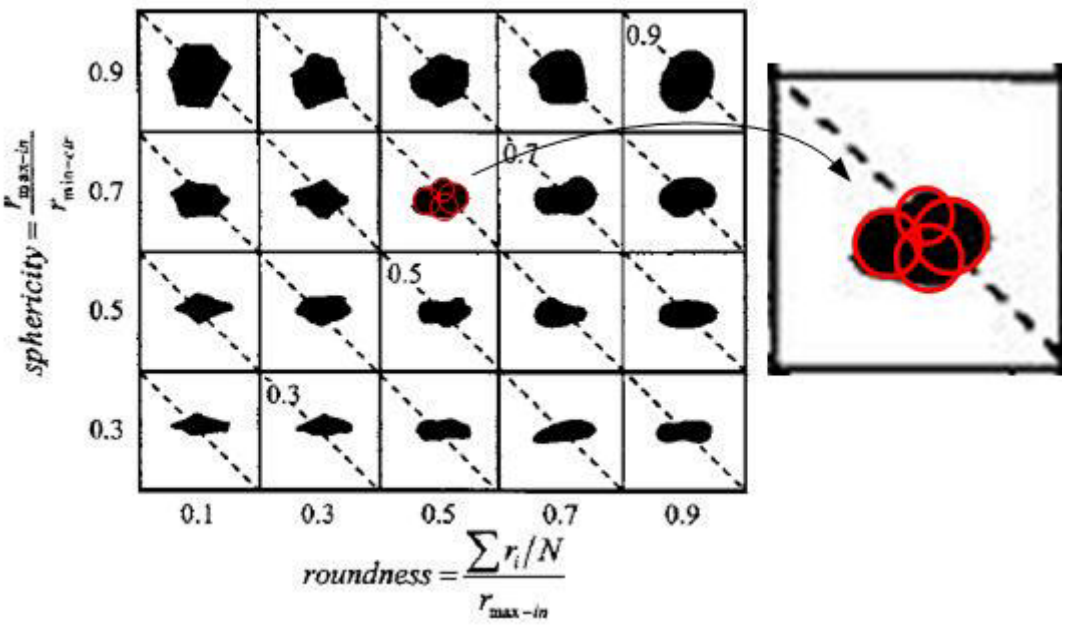


Figure 7.3. Making clumps from the chart that reflect the shape of grain

In order to define a clump completely, radius and x-y coordinates of the circles need to be specified, these are given in Table 7.1. Note that these values are relative within the clump, therefore dimensions are not given. The volume of the clump will be equal to the volume of the ball it replaces. The shapes used for the clumps are given in Figure 7.4.

Table 7.1. Radius, x and y coordinates of clumps

		Radius	x	y
Sile Sand	**Ball 1**	7.5	0.0	4.0
	Ball 2	7.3	10.0	8.0
	Ball 3	6.0	10.0	0.0
	Ball 4	7.5	17.0	7.0
Silivri Sand	**Ball 1**	9.3	0.0	0.0
	Ball 2	6.5	13.0	0.0
	Ball 3	5.5	9.7	8.7
	Ball 4	5.0	3.0	11.0
Crushed Sand	**Ball 1**	7.3	0.0	4.5
	Ball 2	4.0	9.0	8.0
	Ball 3	6.5	7.0	0.0
	Ball 4	6.5	17.0	4.0
Meric Sand	**Ball 1**	8.5	0.0	4.0
	Ball 2	7.5	8.0	11.0
	Ball 3	6.0	9.0	0.0
	Ball 4	8.5	16.0	8.0
Sakarya Sand	**Ball 1**	8.5	0.0	2.0
	Ball 2	8.5	9.0	10.0
	Ball 3	9.0	8.0	0.0
	Ball 4	8.3	17.0	8.0

7.3. Effect of Clump Detail on Angle of Repose Value

Sphericity is mathematically defined as the diameter of the largest inscribed sphere relative to the diameter of the smallest circumscribed sphere (Cho, 2006). The approximate values of sphericity were found for 5 different sand specimens, and this numerical value can also be attached to a clump consisting of two balls. The mathematical formula for sphericity is,

$$S = \frac{R_{\max-\text{in}}}{R_{\min-\text{cir}}} \tag{7.1}$$

where S is sphericity, $R_{\max-\text{in}}$ is the diameter of the largest inscribed circle, and $R_{\min-\text{cir}}$ is the smallest circumscribed circle. If a clump consisting of two identical balls is generated as shown in Figure 7.5, where $R_1 = R_2 = R$, then radius of the minimum circumferential circle will be only dependent on the distance between the centers of the circles pertaining

the clump. If two balls forming the clump is close to each other sphericity will be higher and if they are apart from each other sphericity will be lower.

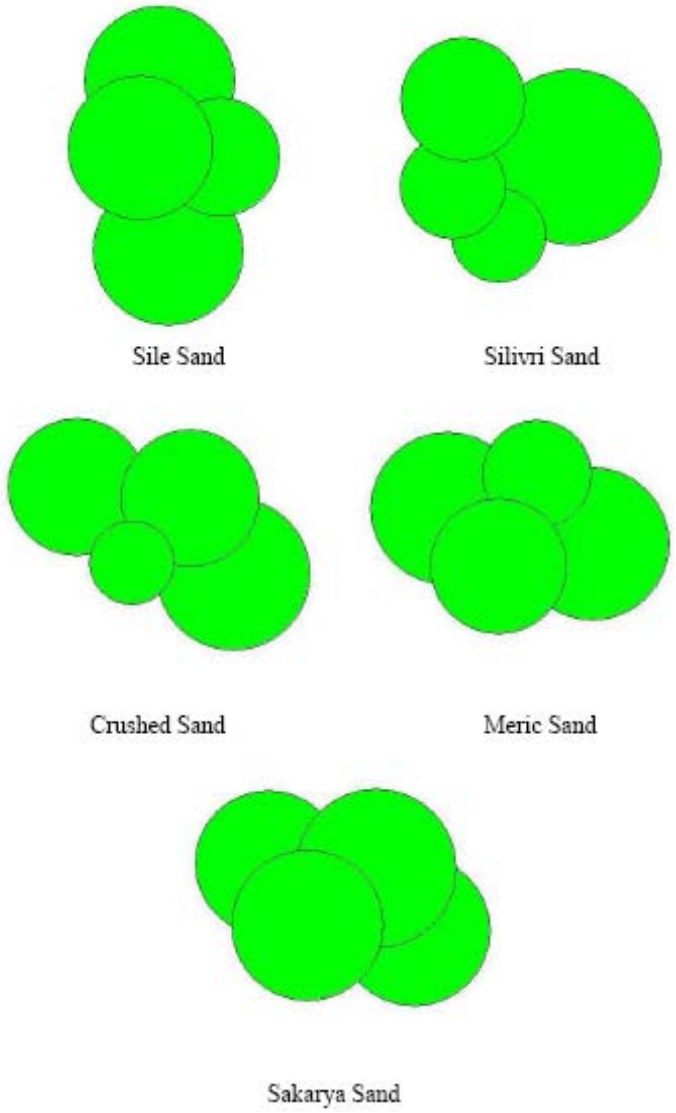


Figure 7.4. Shapes of clumps selected for different types of sands

Two clumps consisting of two identical balls are produced with changing the distance of the centers of identical balls. The relative distance values are given in Figure 7.6. According to these values the sphericity of the clumps are:

$$S_{(\text{clump1})} = \frac{2}{2.5} = 0.8 \tag{7.2}$$

and

$$S_{(\text{clump2})} = \frac{2}{3} = 0.67 \tag{7.3}$$

Clump 1 and clump 2 has the same properties except their sphericity value. By changing the value of sphericity only in the program the effect of it can be examined in the model. In this stage of the study, a comparison is made by running simulations of angle of repose tests on; single ball, clump 1, clump 2, and clump of Sile sand.

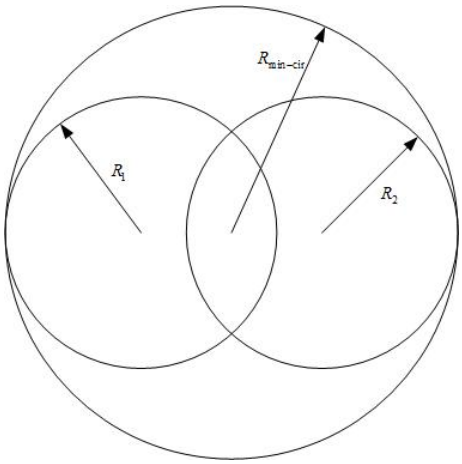


Figure 7.5. Clump consists of two balls

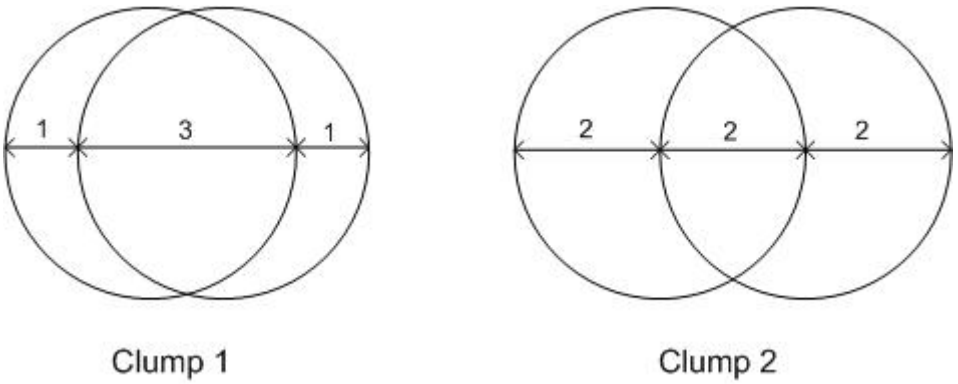


Figure 7.6. Two different clumps consist of two identical balls

Different heaps are formed and different values of angle of repose are obtained after running the numerical test. The graphical output of the program and the results are

shown in Figure 7.7. The coefficient of friction, $\mu = 0.6$ is selected same for the ball and clumps to eliminate its effect.

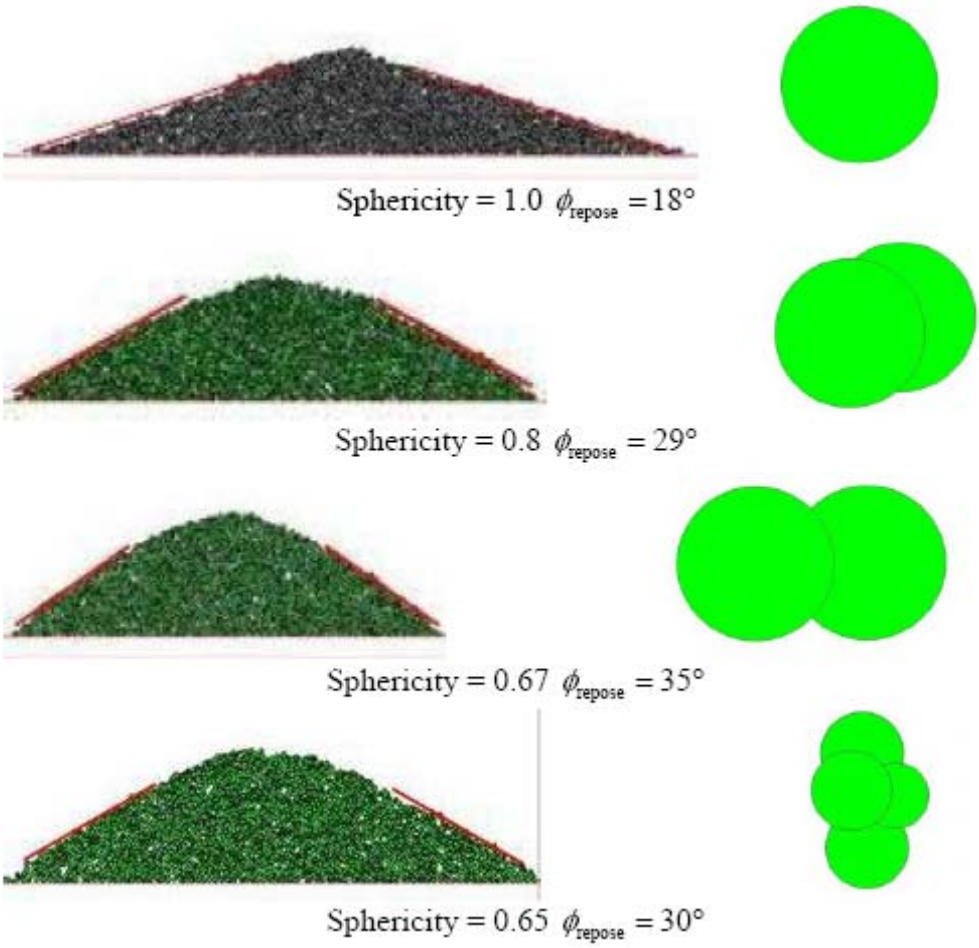


Figure 7.7. Results of numerical angle of repose test on different clumps

Comparing the results from the ball, clump 1, and clump 2 we can say that angle of repose increases as sphericity decreases, as expected. A single ball represents a situation of perfect roundness, whereas clumps consisting of two balls with different center to center distance represent two different grains which have different sphericity values. As a result it can be said that the effect of sphericity on angle of repose value is confirmed for the model.

Comparing the result of clump 1 and Sile sand, we can see that nearly same angle of repose values are obtained with different sphericity values. The sphericity value of

clump 1 is 0.8 and the sphericity value of clump representing the shape of Sile sand is 0.65. The angle of repose values obtained for clump 1 and Sile sand is 29° and 30° respectively. Therefore it can be said that representation of shape is different than representation of sphericity of the grain.

Comparing results of clump 2 and Sile sand, we can see that different angle of repose values are obtained with nearly same sphericity value. The sphericity value of clump 2 is 0.67 and the sphericity value of Sile sand is 0.65. The angle of repose values are 35° for clump 2 and 30° for Sile sand. Clumps with nearly same sphericity value gives different angle of repose values. Again it can be said that representation of shape gives different values than representation of sphericity only.

As a result, it can be concluded that generating clumps using as much balls as possible will represent the shape effect more efficiently. Any sphericity value can be obtained using two balls as a clump because sphericity is only related with the height and width of the grain in two dimensions. Representation of angularity is not possible combining balls together in a clump because balls themselves are not angular. Angularity is a property related to the surface features of the grains. Increasing the number of balls used in one clump changes the surface shape of the grain therefore it may reflect the angularity of a grain not completely but in a manner. The results support that it is logical to represent the grain shape qualitatively. More representative values may be obtained if more balls are used in one clump, but runtime will be much longer. The idea of the modeling is to represent the real situation as simple as possible with providing essential features.

7.4. Modeling of Different Sand Specimens Using Clumps Containing Four Balls

At the last stage of distinct element modeling of angle of repose test, the grain shapes are included in the model by generating clumps consist of four balls. The representation of grain shape is directly proportional with the number of balls used in one clump. A single clump in the model is the equivalent of a single grain in reality. Two set of numerical experiments are conducted, first for uniformly graded sand, and second for well

graded sand. The gaps of the volume of clumps are determined considering the particle size distribution for uniform grading and well grading.

In PFC2D program, 2000 balls are used for uniformly graded sand and 1251 balls are used for well graded sand. These balls are replaced by clumps of equal volume. The diameter of the balls replaced by clumps in the program PFC2D was linearly distributed between the opening sizes of sieves. For example, the uniformly graded sand sample was retained between sieves No. 16 and No. 40. The respective opening sizes of sieves are 0.42 mm and 1.19 mm. In the program, minimum radius value for a ball is given as 0.42 mm and maximum value of ball radius is given as 1.19 mm. Thus, 2000 balls have different radius values between 0.42 and 1.19. The purpose is to model the grading of the specimens.

The value of angle of repose is found using the same method applied for laboratory tests. A line is drawn to the slope forming after the pluviation of sand grains (Figure 7.8). The angle between horizontal axis and red line drawn is measured and this is the angle of repose value for the numerical experiment. For the comparison of interparticle friction coefficient with material friction angle, different values of friction coefficients are given to the balls forming the clumps. Comparing the values of angle of repose obtained from laboratory experiments and numerical experiments the model value of interparticle friction coefficient is calibrated.



Figure 7.8. Obtaining angle of repose value from numerical experiment

Table 7.2 and Figure 7.9 shows angle of repose values for uniformly graded sand specimens obtained for different interparticle friction coefficients assigned to clumps. Trials result in a conclusion that a value between 0.8 and 0.9 generally give close results to the findings of laboratory experiment.

Table 7.2. Values obtained from uniformly graded sand specimens

Uniformly Graded Sand between No. 16 and No. 40 Sieves					
Interparticle Friction Coefficient	**Sile Sand**	**Silivri Sand**	**Crushed Sand**	**Meric Sand**	**Sakarya Sand**
0.5	29.5	25	33.5	30.5	30
0.6	30	26	35	32	31.5
0.7	30.5	28	35.5	33	32
0.8	30.5	31	36	34.5	34
0.9	31	32	37.5	38	35
Experimental Value	31	31.5	36.5	36	34

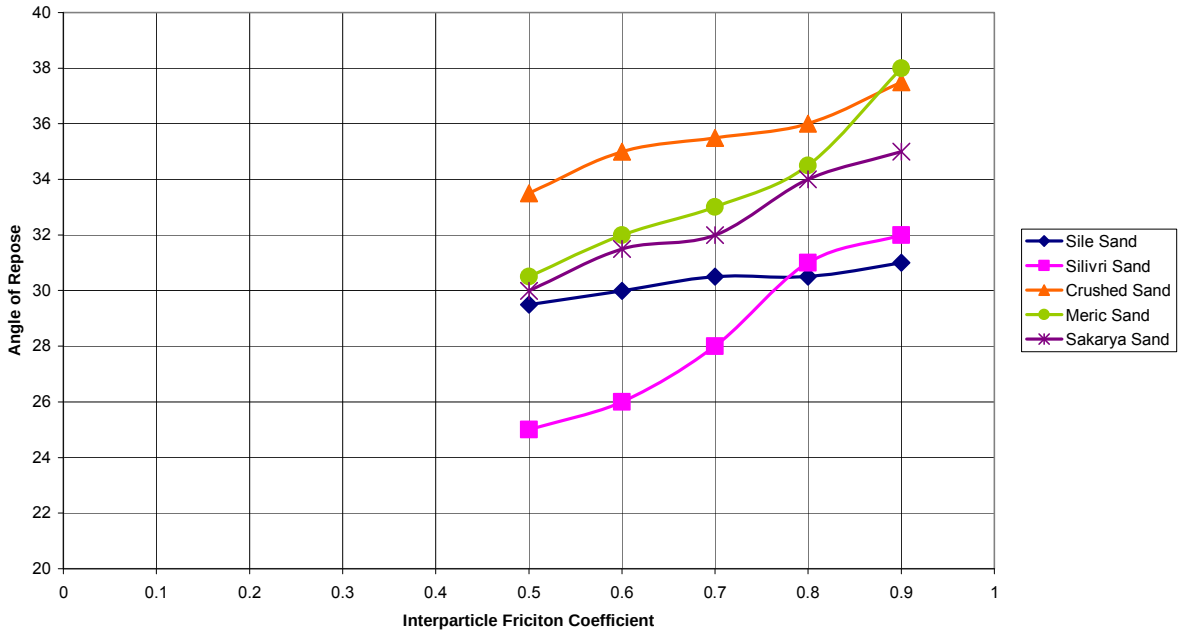


Figure 7.9. Angle of repose vs. interparticle friction coefficient for uniformly graded sands

Table 7.3 and Figure 7.10 shows angle of repose values for well-graded sand specimens obtained for different interparticle friction coefficients assigned to clumps. Trials result in a conclusion that a value between 0.5 and 0.6 generally give close results to the findings of laboratory experiment.

Different interparticle friction coefficients are found for uniformly graded soils and well graded soils. An average value of interparticle friction coefficient of 0.85 and 0.52 are found for uniformly graded sand and well graded sand respectively. Particle size distribution is maintained in the model by using radius variations reflecting the grading of the soil specimens. Particle shape is also maintained by using different clumps for different

sand types. Therefore it was expected that the interparticle friction coefficient values obtained be the same for uniformly graded and well graded sands since there was no change in the properties of clumps except the radius values. The estimated cause of the difference in the interparticle friction coefficient values of uniformly graded and well graded sand is related to percolation. In PFC2D small particles can easily percolate through a 3D assembly comprised of larger particles, but they can never percolate through a packed PFC2D model, regardless of relative particle sizes.

Table 7.3. Values obtained from well-graded sand specimens

Well Graded Sand between No. 10 and No. 70 Sieves					
Interparticle Friction Coefficient	**Sile Sand**	**Silivri Sand**	**Crushed Sand**	**Meric Sand**	**Sakarya Sand**
0.4	30	31	35	35	31
0.5	30.5	33.5	36.5	36	33
0.6	34	33	37	37	35
0.7	35	36	38	41	36
0.8	36	36.5	38.5	41.5	38.5
0.9	37	40	41	42	40
Experimental Value	32	35	36.5	35	34.5

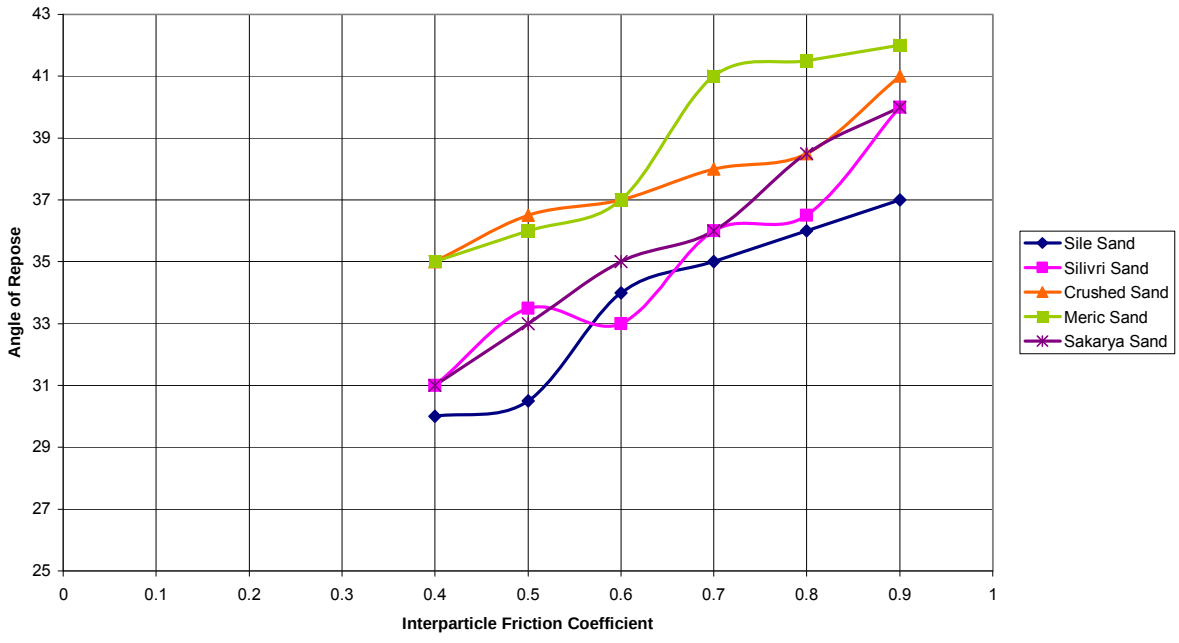


Figure 7.10. Angle of repose vs. interparticle friction coefficient for well-graded sands

From the results obtained from comparison of numerical and laboratory experiments on angle of repose, interparticle friction coefficient can be taken between 0.8 and 0.9 for uniformly graded soils, and between 0.5 and 0.6 for well graded soils. These values may be used when modeling in 2D. Percolation problem should be kept in mind.

8. RESULTS AND DISCUSSION

The results of angle of repose experiments are tabulated in Table 8.1. Angle of repose values are nearly the same for uniformly graded and well graded condition. Only there is an increase at the value of angle of repose for Silivri Sand, but for the others differences are minimal.

Table 8.1. Results of angle of repose experiment

	Angle of Repose (°)	
	Uniformly Graded	Well Graded
	Between sieves No. 16 and No. 40	Between Sieves No.10 and No. 70
Sile Sand	31	32
Silivri Sand	31.5	35
Crushed Sand	36.5	36.5
Meric Sand	36	35
Sakarya Sand	34.5	34.5

The angle of repose test is modeled in distinct element program PFC2D, for finding the relationship between continuum friction angle and interparticle friction coefficient. The increase in interparticle friction coefficient increases the angle of repose for uniformly graded sand (Figure 8.1). The value of interparticle friction coefficient for exactly obtaining the experimental results is tabulated in Table 8.2. The average of the values of interparticle friction coefficient is found to be 0.85. All values lie within 0.8 and 0.9, therefore it can be said that for uniformly graded soils these values represent the interparticle friction angle.

The model is also created for well graded sand. An average value of 0.517 is obtained for well graded sands using distinct element modeling. The values deviate between 0.4 and 0.67, in a larger gap than uniformly graded sands.

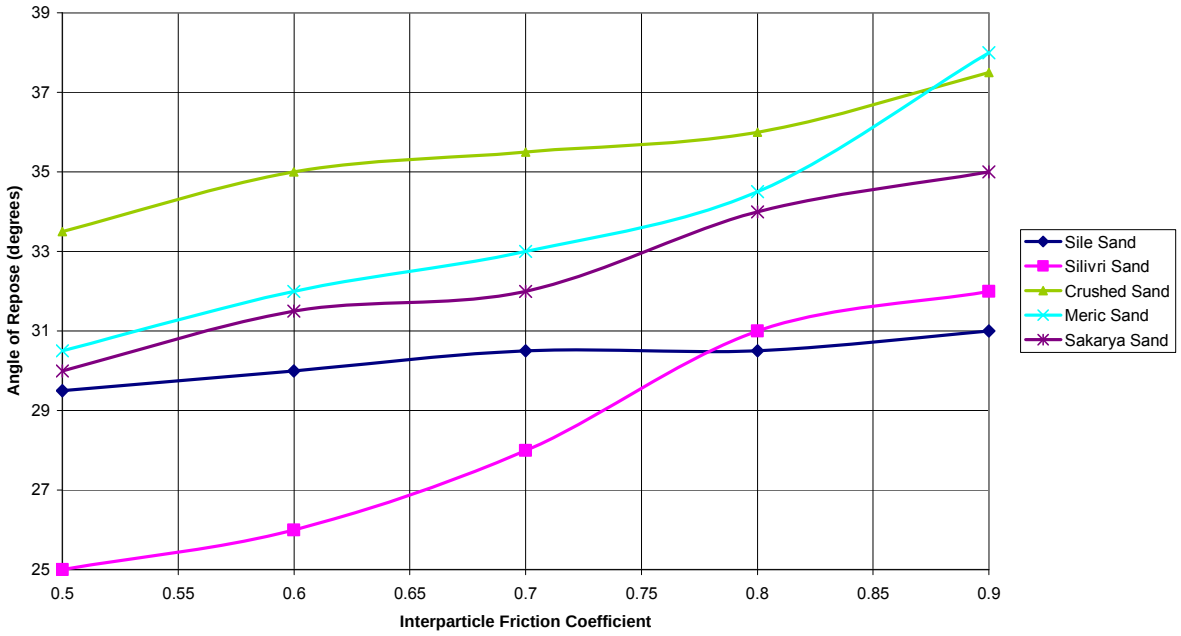


Figure 8.1. Change in angle of repose values with interparticle friction coefficient for uniformly graded sand

Table 8.2. Interparticle friction coefficients giving the same results as experiments for uniformly graded sands

Uniformly Graded	Interparticle friction coefficient giving the same result as the experiment	Angle of Repose value obtained experimentally
Sile Sand	0.900	31.0
Silivri Sand	0.850	31.5
Crushed Sand	0.833	36.5
Meric Sand	0.843	36.0
Sakarya Sand	0.800	34.0

The difference in the coefficient of interparticle friction coefficient between uniformly graded sand and well graded sand in the numerical models is an inconsistent situation. The reason of this situation is related with the percolation problem. Small particles can not percolate through the voids in 2D model, as in real case, therefore smaller intergranular friction coefficients are obtained for well graded soils. The displacements of small sized particles are blocked by larger sized particles when there is significant difference between the sizes of the clumps.

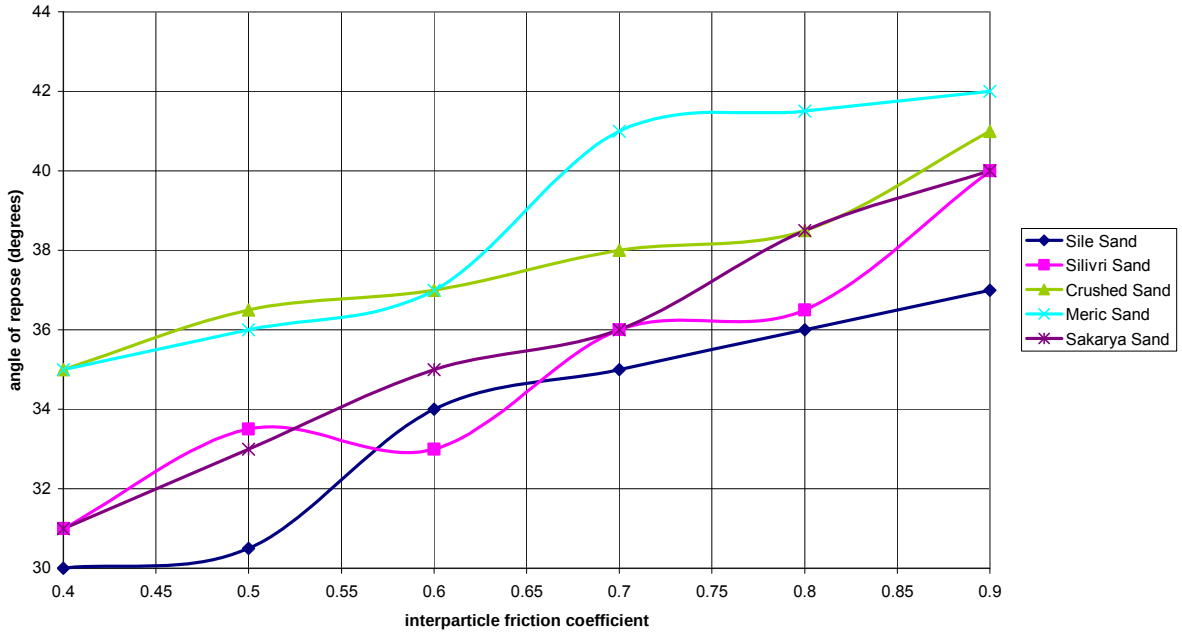


Figure 8.2. Angle of repose values for different interparticle friction coefficient for well graded sands

Table 8.3. Interparticle friction coefficients giving the same results as experiments for well graded sands

Well Graded	Interparticle friction coefficient giving the same result as the experiment	Angle of Repose value obtained experimentally
Sile Sand	0.443	32.0
Silivri Sand	0.667	35.0
Crushed Sand	0.500	36.5
Meric Sand	0.400	35.0
Sakarya Sand	0.575	34.5

Numerical models are reflections of the real situation constructed using simplified assumptions. For example in sands the number of particles and the number of interactions at contact points are dauntingly high, therefore it is impossible to include all of the particles in the model. Therefore, number of particles included in the model is reduced in comparison to real problem. The computer runtime is directly proportional with the number of particles used in the model. The same problem arises when representing the grain shapes of particles. Grain shapes are represented in the model by attaching ball

shaped particles together which are called clumps to obtain particles having different surface shape. If the number of balls used to construct a single clump is increased, the shape is represented better. The decision of number of particles used in a single clump and number of clumps used to construct the assembly is a matter of runtime. This can be considered as an optimization problem. The number of particles that can be used in the model and the number of balls that can be used in a single clump is limited with the computational power.

9. CONCLUSION

In this study, a new method for obtaining a representative value for the coefficient of friction used in Discrete Element Method is proposed. This is important to correctly reflect the behavior of granular media in DEM. In soil mechanics, the shear strength of granular materials like sands is examined using laboratory experiments. In all of these tests like direct shear test, simple shear test, angle of repose test, triaxial test representative samples obtained from field are used. The scales of the tests are small compared to field, but still there are dauntingly high numbers of grains in even the smallest samples used in soil mechanics laboratory testing. Therefore, the samples are examined at macro scale, and as a continuous media. However, when they are treated as continuous materials, grain-to-grain interactions are ignored. In continuum mechanics approach, two most important properties of sands that determine the shear strength are known to be void ratio and confining stress. In addition to them, the properties like size, shape, and roughness of the particles also contribute to the shear strength of sands, but they are not taken into account in continuum mechanics approach. One of these parameters, the roughness, which determines the intergranular friction coefficient between contacting grains, is investigated in this study by numerical modeling of angle of repose test using distinct element method.

In this study, in order to obtain the coefficients of friction for different sand samples the following tests are conducted. Different sand specimens are separated into grades by wet sieving technique. Specific gravity of soil solids are determined by the help of water pycnometer. The grain photographs of individual grains are taken and shape parameters (roundness and sphericity) are determined using the particle shape determination chart taken from the study of Cho et al. (2006). Shear strengths of sands are found by conducting angle of repose test on dry sand specimens in uniformly graded and well graded conditions. After these works, the grading, density of soil solids, shape parameters, and shear strength are known parameters for numerical modeling. The PFC2D (Particle Flow Code in 2D) is used to construct a numerical model for the angle of repose test. The grading of the material is maintained by giving different radius values to the balls. Also specific gravity values are used to give appropriate density values to the balls representing grains. The shapes of the grains are included into the model by attaching balls

together to form clumps. The test conditions are simulated by direct pluviation of the clumps from a specified distance as in the real laboratory experiment. The only remaining parameter to construct the model is the intergranular coefficient of friction, which is the unknown, and the parameter that is investigated in this study.

The output obtained from the numerical model is a formation of slope consisting of clumps. The angle of repose can be measured with the help of a compass as in the laboratory experiment. A range of intergranular friction coefficient values are given to the clumps and the obtained results are compared. The values that give the same results as the experiments are founded. For the uniformly graded condition values ranging between 0.8 and 0.9 is found representative, while values between 0.4 and 0.67 were reflected the real situation for well graded condition. The cause of the difference is found to be the percolation problem. Small particles can not percolate through the voids in 2D model, while they can in real 3D situation.

Another thing that should be taken into account is about the detail level included in the model. Selecting number of balls used in a single clump and number of clumps constituting the assembly is a decision depending on the computer power and time. Computer runtime is the limiting factor in discrete element modeling. The model should contain the characteristic features that are essential in the context of the problem to be solved or described. By adding more detail to the model, more representative results will be obtained.

REFERENCES

American Society for Testing and Materials, 1998, "Standard Practice for Wet Preparation of Soil Samples for Particle Size Analysis and Determination of Soil Constants", *ASTM Standards: D2217*.

American Society for Testing and Materials, 2005, *ASTM Book of Standards*, Section 4, Vol. 04.08, West Conshohocken, Pa.

American Society for Testing and Materials, 2006, "Standard Test Methods for Specific Gravity of Soil Solids by Water Pycnometer", *ASTM Standards: D854*.

American Society for Testing and Materials, 2007, "Standard Test Method for Unconsolidated-Undrained Triaxial Compression Test on Cohesive Soils", *ASTM Standards: D2850*.

American Society for Testing and Materials, 2009, "Standard Specification for Woven Wire Test Sieve Cloth and Test Sieves", *ASTM Standards: E11*.

Bardet, J. P., 1997, *Experimental Soil Mechanics*, Prentice Hall, New Jersey.

Barrett, P. J., 1980, "The Shape of Rock Particles, a Critical Review", *Sedimentology,* Vol. 27, pp. 291–303.

Bathurst, R. J. and L. Rothenburg, 1988, "Micromechanical Aspects of Isotropic Granular Assemblies with Linear Contact Interactions", *Journal of Applied Mechanics*, Vol. 55, pp. 17–23.

Calvetti F., G. Combe and J. Lanier, 1997, "Experimental Micromechanical Analysis of a 2D Granular Material: Relation Between Structure Evolution and Loading Path", *Mechanics of Cohesive Frictional Materials*, Vol. 2, pp. 121–163.

Carrigy M., 1970, "Experiments on the Angles of Repose of Granular Materials", *Sedimentology*, Vol. 14, pp. 147–158.

Cho C. G., J. Dodds and J. C. Santamarina, 2006, "Particle Shape Effects on Packing Density, Stiffness and Strength: Natural and Crushed Sands", *Journal of Geotechnical and Geoenvironmental Engineering*, Vol. 132, pp. 591–602.

Craig, R. F., *Soil Mechanics*, Spon Press, London and New York, 2004.

Cundall P. A. and O. D. L. Strack, 1979, "A Discrete Numerical Model for Granular Assemblies", *Geotechnique*, Vol. 29, pp. 47–65.

Cundall, P. A., 1971, "A Computer Model for Simulating Progressive Large Scale Movements in Blocky Rock Systems", *Proceedings of the Symposium of the International Society of Rock Mechanics*, Vol. 1, No. II-8, Nancy, France.

Cundall, P. A., 1988, "Formulation of a Three-Dimensional Distinct Element Model Part I. A Scheme to Detect and Represent Contacts in a System Composed of Many Polyhedral Blocks", *Int. J. Rock Mech., Min. Sci. & Geomech. Abstr.*, Vol. 25, pp. 107–116.

Cundall, P. A. and R. Hart, 1992, "Numerical Modeling of Discontinua", *J. Engr. Comp.*, Vol. 9, pp. 101–113.

Ghazavi, M., M. Hosseini and M. Mollanouri, 2008, "A Comparison Between Angle of Repose and Friction Angle of Sand", *The 12th International Conference of International Association for Computer Methods and Advances in Geomechanics (IACMAG)*, India.

Hart, R., P.A. Cundall and J. Lemos, 1988, "Formulation of a Three-Dimensional Distinct Element Model – Part II. Mechanical Calculations for Motion and Interaction of a System Composed of Many Polyhedral Blocks", *Int. J. Rock Mech., Min. Sci. & Geomech. Abstr.*, Vol. 25, pp. 117–125.

Head. K. H., 1984, *Manual of Soil Laboratory Testing, Vol. 1*, Pentech Press, London.

Huang, Z., Z. Yang and Z. Wang, 2008, "Discrete Element Modeling of Sand Behavior in a Biaxial Shear Test", *Journal of Zhejiang University Science A*, Vol. 9, pp. 1176–1183.

Itasca Consulting Group, 2008, *PFC2D (Particle Flow Code in 2 Dimesions) User Manuals Version 4.0.* , Minneapolis: ICG.

Jørgensen, S.E., H.T. Tsuno, H. Mahler and V. Santiago, 2003, *PAMOLARE Training Package, Planning and Management of Lakes and Reservoirs: Models for Eutrophication Management*, UNEP DTIE IETC and ILEC, 1091 Oroshimo-cho, Kusatsu, Shiga, 525-0001, Japan.

Kadau D., D. Schwesig, J.T. Dietrich and E. Wolf, 2006, "Influence of Particle Elasticity in Shear Testers", *Granular Matter*, Vol. 8, pp.35–40.

Krumbein, W. C., 1941, "Measurement and Geological Significance of Shape and Roundness of Sedimentary Particles", *J. Sediment. Petrol*, Vol. 11, pp. 64–72.

Lambe, T. W. and R. V. Whitman, 1969, *Soil Mechanics*, John Wiley & Sons, New York.

Margolis S. V., D. H. Krinsley, 1974, "Processes of Formation and Environmental Occurence of Microfeatures on Detrital Quartz Grains", American Journal of Science, Vol. 274, pp. 449–464.

Miura, K., K. Maeda and S. Toki, 1997, "Method of Measurement for the Angle of Repose of Sands", *Soils and Foundations*, Vol. 37, pp. 89–96.

Moore, D. S. and G.P. McCabe, 2003, *Introduction to the Practice of Statistics*, 4th edition, W. H. Freeman and Company, New York.

Mustoe, G. G. W. and M. Miyata, 2001. "Material Flow Analyses of Noncircular Shaped Granular Media Using Discrete Element Method", *Journal of Engineering Mechanics*, Vol. 127, 10,pp. 1017–1026.

Oner M., 1984, "Analysis of Fabric Changes During Cyclic Loading of Granular Soils", *Proc. 8th World Conf. Earthquake Engineering*, San Francisco, Calif., Vol. 3, pp. 55–62.

Pohlman A. N., B.L. Severson, J. M. Ottino and R. M. Lueptow, 2006, "Surface Roughness Effects in Granular Matter: Influence on Angle of Repose and the Absence of Segregation", *Physical Review E*, Vol. 73, 031304.

Rahaman M. N., 1995, *Ceramic Processing and Sintering*, Dekker, New York.

Rouse, P. C., R. J., Fannin and D. A. Shuttle, 2008, "Influence of Roundness on the Void Ratio and Strength of Uniform Sand", *Geotechnique,* Vol. 58, pp. 227–231.

Santamarina, C. and G. Cascante, 1998, "Effect of Surface Roughness on Wave Propagation Parameters", *Geotechnique*, Vol. 48, pp. 129–136.

Skinner, A. E., 1969, "A Note on the Influence of Interparticle Friction on the Shearing Strength of a Random Assembly of Spherical Particles", *Geotechnique*, Vol. 19, pp. 150–157.

Ting, J. M., B. T. Corkum, C. R. Kauffman and C. Greco, 1989, "Discrete Numerical Model for Soil Mechanics", *Journal of Geotechnical Engineering*, Vol. 115.

Vaid, Y. P. and D. Negussey, 1988, "Preparation of Reconstituted Sand Specimens", *Advanced Triaxial Testing of Soil and Rock, ASTM STP 977*, American Society for Testing Materials, Philedelphia, pp. 405–417.

Wadell, H., 1932, "Volume, Shape and Roundness of Rock Particles", *Journal of Geology*, Vol. 40, pp. 443–451.

Zhang, Y. and P. A. Cundall, 1986, "Numerical Simulation of Slow Deformations", *Proc. Symp. on the Mechanics of Particulate Media, 10th National Congress on Applied Mechanics*, Austin, Texas.

Zhou, Y. C., B. H. Xu and A. B. Yu, 2001, "Numerical Investigation of Angle of Repose of Monosized Spheres", *Physical Review E*, Vol. 64, 021301.